

The cosmological properties of AGN in the XMM-Newton Hard Bright Survey

R. Della Ceca¹, A. Caccianiga¹, P. Severgnini¹, T. Maccacaro¹, H. Brunner², F. J. Carrera³, F. Cocchia^{1,4}, S. Mateos⁵, M.J. Page⁶, and J.A. Tedds⁵

¹ Istituto Nazionale di Astrofisica (INAF), Osservatorio Astronomico di Brera, Via Brera 21, 20121 Milano, Italy
e-mail: roberto.dellaceca@brera.inaf.it

² Max-Planck-Institut für extraterrestrische Physik, Giessenbachstrasse, 85741 Garching, Germany

³ Instituto de Física de Cantabria (CSIC-UC), Avenida de los Castros, 39005 Santander, Spain

⁴ INAF - Osservatorio Astronomico di Roma, via di Frascati 33, 00040 Monte Porzio Catone, Italy

⁵ X-ray & Observational Astronomy Group, Department of Physics and Astronomy, Leicester University, Leicester LE1 7RH, UK

⁶ Mullard Space Science Laboratory, University College London, Holmbury St. Mary, Dorking, Surrey, RH5 6NT, UK

Received: December 26, 2007; accepted: April 28, 2008

ABSTRACT

Aims. We investigate here the X-ray luminosity function (XLF) of absorbed (N_H between 4×10^{21} and 10^{24} cm^{-2}) and unabsorbed ($N_H < 4 \times 10^{21}$ cm^{-2}) AGN, the fraction of absorbed AGN as a function of L_X (and z), the intrinsic N_H distribution of the AGN population, and the XLF of Compton Thick ($N_H > 10^{24}$ cm^{-2}) AGN.

Methods. To carry out this investigation we have used the XMM-Newton Hard Bright Serendipitous Sample (HBSS) a complete sample of bright X-ray sources ($f_x \gtrsim 7 \times 10^{-14}$ $\text{erg cm}^{-2} \text{ s}^{-1}$) at high galactic latitude ($|b| > 20^\circ$) selected in the 4.5-7.5 keV energy band. The HBSS sample is now almost completely identified (97% spectroscopic identifications) and it can be safely used for a statistical investigation. The HBSS contains 62 AGN out of which 40 are unabsorbed (or marginally absorbed; $N_H < 4 \times 10^{21}$ cm^{-2}) and 22 are absorbed (N_H between 4×10^{21} and $\sim 10^{24}$ cm^{-2}).

Results. Absorbed and unabsorbed AGN are characterized by two different XLF with the absorbed AGN population being described by a steeper XLF, if compared with the unabsorbed ones, at all luminosities. The intrinsic fraction F of absorbed AGN (i.e. the fraction of sources with N_H between 4×10^{21} and 10^{24} cm^{-2} divided the sources with N_H below 10^{24} cm^{-2} , corrected for the bias due to the photoelectric absorption) with $L_{2-10\text{keV}} \gtrsim 3 \times 10^{42}$ erg s^{-1} is 0.57 ± 0.11 ; we find that F decreases with the intrinsic luminosity, and probably, increases with the redshift. Our data are consistent with a flat $\text{Log } N_H$ distribution for N_H between 10^{20} and 10^{24} cm^{-2} . Finally, by comparing the results obtained here with those obtained using an optically selected sample of AGN we derive, in an indirect way, the XLF of Compton Thick AGN; the latter is well described by a XLF similar, in shape, to that of absorbed AGN but having a normalization about a factor 2 above. The density ratio between Compton Thick AGN ($N_H \gtrsim 10^{24}$ cm^{-2}) and Compton Thin AGN ($N_H \lesssim 10^{24}$ cm^{-2}) decreases from 1.08 ± 0.44 at $\sim 10^{43}$ erg s^{-1} to 0.57 ± 0.22 at $\sim 10^{44}$ erg s^{-1} to 0.23 ± 0.15 at $\sim 10^{45}$ erg s^{-1} .

Conclusions. The results presented here on the anti-correlation between F and $-L_x$ are fully consistent with the hypothesis of a reduction of the covering factor of the gas as a function of the luminosity and are clearly inconsistent with the simplest unified scheme of AGN. These results strongly support the recently proposed radiation-limited dusty torus model although alternative physical models are also consistent with the observations.

Key words. galaxies: active – galaxies: nuclei – galaxies: evolution – X-ray: diffuse background – X-ray: Surveys – X-ray: active galaxies

1. Introduction

For many years the study of the cosmological and statistical properties (e.g. luminosity function, cosmological evolution, mean spectral properties) of Active Galactic Nuclei (AGN) was principally limited to the optical (see e.g. Boyle et al. 1988; Croom et al. 2004) or soft X-rays (see e.g. Maccacaro et al. 1991, Della Ceca et al. 1992, Miyaji et al. 2001, Hasinger et al.

2005) bands and essentially dealt with complete and unbiased samples of optically unabsorbed (type 1) AGN. Indeed the selection and identification of sources hosting obscured accreting nuclei is a difficult task: in the optical domain the active nuclei appear very dim and their luminosity could be comparable to that of their host galaxies, while in the soft X-ray band (up to few keV) their selection is difficult since even hydrogen column densities (N_H) of the order of 10^{21} - 10^{22} cm^{-2} strongly reduce the flux from the nuclear source.

However, despite their elusiveness, obscured AGN are fundamental for our understanding of the Super-Massive Black Holes (SMBHs) history as the large majority of the energy density generated by accretion of matter in the Universe seem to take place in obscured AGN (Fabian et al. 1998), as testified by the integrated energy density contained in the cosmic X-ray background (XRB; Setti and Woltjer 1989; Madau et al. 1994; Comastri et al. 1995; Gilli et al. 2007). Even more important, the recent discovery of quiescent SMBH in the nuclei of non-active nearby galaxies with prominent bulges (Kormendy & Richstone 1995, Magorrian et al. 1998), along with the presence of scaling relations between the central BH mass and galaxy properties (e.g. bulge luminosity/mass and velocity dispersion, Ferrarese & Merritt 2000) strongly suggest that AGN are leading actors in the formation and evolution of galaxies and, in general, of cosmic structures in the Universe (see Begelman 2004 and references therein). Missing a large fraction of the AGN population could thus bias our understanding of the evolution of cosmic structure in the Universe.

Hard X-rays (photon energies between a few keV and ~ 10 keV) can directly probe AGN activity, since they are almost uncontaminated by star formation processes at the X-ray luminosities of interest ($L_X \gtrsim 10^{42}$ erg s $^{-1}$), and they are sensitive to absorbed AGN up to an intrinsic absorbing column density of $N_H \sim 10^{23.5-24}$ cm $^{-2}$, that is to say, they detect all but the most absorbed sources. Thus, hard X-ray surveys in the 2-10 keV range, as pioneered by ASCA and BeppoSAX (Cagnoni et al. 1998; Ueda et al. 1998; Della Ceca et al. 1999; Fiore et al. 1999; Ueda et al. 2003), and now routinely performed with *Chandra* and *XMM-Newton*¹, provide among the most complete and unbiased samples of AGN presently possible (although they still miss Compton Thick sources i.e. the sources with absorbing column densities $\gtrsim 10^{24}$ cm $^{-2}$). In spite of this, a significant fraction of the AGN found in medium and deep fields is too faint to provide good X-ray spectral information. Furthermore, the extremely faint magnitudes of a large number of optical counterparts of these X-ray faint sources make the spectroscopic identifications very difficult, or even impossible, with the present day ground-based optical telescopes.

Here we use the bright ($f_X \gtrsim 10^{-13}$ erg cm $^{-2}$ s $^{-1}$), hard (4.5-7.5 keV selection band), almost completely identified (97% spectroscopic ID) XMM-Newton Hard Bright Sample, to discuss a few issues which are currently subject of intense research activity, namely: a) the statistical properties (e.g. X-ray luminosity functions) of absorbed and unabsorbed AGN; b) the intrinsic ratio of absorbed and unabsorbed AGN as a function of the X-ray luminosity; c) the intrinsic absorption column density distribution of the AGN population for Hydrogen column density up to $\sim 10^{24}$ cm $^{-2}$ and d) the X-ray luminosity function of Compton Thick AGN. These are fundamental issues both to study and to follow the accretion history in the Universe and to test the unification models of AGN. We stress that the high identification rate of the HBSS sample is fundamental to in-

vestigate these issues since interesting and important classes of X-ray emitting sources (e.g. the type 2 QSOs) could be more difficult to identify and therefore could be under-represented even in samples with an identification rate of the order of 90%. Furthermore, good optical and X-ray spectral data are available for almost all the sources in the HBSS sample. In particular the results of a complete X-ray spectral analysis will be efficiently used here to separate absorbed AGN from the unabsorbed ones and to compute k-corrections.

This paper is organized as follows: in §2 we give a short account of the XMM-Newton Bright Serendipitous Survey and a description of the AGN sample selected in the 4.5-7.5 keV range (the HBSS AGN sample hereafter). In §3 we study the cosmological evolution properties of the HBSS AGN sample and derive the X-ray luminosity function (XLF) of the total AGN population as well as the XLF of absorbed and unabsorbed AGN separately. The intrinsic fraction of absorbed AGN as a function of the X-ray luminosities is discussed in §4, while in §5 we discuss the intrinsic N_H distribution of the AGN population. In §6 we compare our results with the prediction of AGN unification models. In §7 we compare our results on the intrinsic fraction of absorbed AGN as a function of luminosity with those obtained using an optically selected sample of AGN; this comparison will be used to estimate the luminosity function of Compton Thick AGN and to derive the ratio between Compton Thick and Compton Thin AGN as a function of L_X . Finally, summary and conclusions are reported in §8. In Appendix A we discuss the method used to take into account the photoelectric absorption in the computation of the luminosity functions. Throughout this paper we consider the cosmological model with $(H_0, \Omega_M, \Omega_\Lambda) = (65, 0.3, 0.7)$; results from other papers have been rescaled to this cosmological framework.

2. The XMM-Newton Bright Serendipitous Survey and the HBSS AGN Sample

The XMM-Newton Hard Bright Serendipitous Sample used here is part of a bigger survey project known as XMM-Newton Bright Serendipitous Survey² (XBS hereafter). This latter consists of two flux-limited serendipitous samples of X-ray selected sources at high galactic latitude ($|b| > 20^\circ$): the XMM BSS sample (389 sources) and the XMM HBSS sample (67 sources, with 56 sources in common with the BSS sample) having an EPIC MOS2 count rate limit, corrected for vignetting, of 10^{-2} cts/s (2×10^{-3} cts/s) in the 0.5–4.5 keV (4.5–7.5 keV) energy band; the flux limit is $\sim 7 \times 10^{-14}$ erg cm $^{-2}$ s $^{-1}$ in both energy selection bands. At the time of this writing the spectroscopic identification rate is 87% for the BSS sample and 97% for the HBSS sample. The details on the XMM-Newton fields selection strategy and the source selection criteria of the XMM

² The XMM-Newton Bright Serendipitous Survey is one of the research programs conducted by the XMM-Newton Survey Science Center (SSC, see <http://xmmssc-www.star.le.ac.uk>) a consortium of 10 international institutions, appointed by ESA to help the SOC in developing the software analysis system, to pipeline process all the XMM-Newton data, and to exploit the XMM serendipitous detections. The *Osservatorio Astronomico di Brera* is one of the Consortium Institutes.

¹ A compilation of the main extragalactic surveys executed with *Chandra* and *XMM-Newton* is reported at the web address <http://cxc.harvard.edu/xraysurveys/>

BSS and HBSS samples are discussed in Della Ceca et al. (2004) while a description of the optical data and analysis, of the optical classification scheme and of the optical properties of the extragalactic sources identified so far is presented in Caccianiga et al. (2008). The optical and X-ray properties of the galactic population are discussed in López-Santiago et al. (2007).

Since the HBSS sample is now almost completely identified it will be used in this paper for a statistical investigation. We note that among the ongoing surveys performed with *Chandra* and XMM-Newton, the HBSS is currently covering one of the largest area ($\sim 25 \text{ deg}^2$) and, unlike deep pencil beam surveys, is unbiased by problems connected to the cosmic variance. The current classification breakdown of the HBSS sample is as follows: 62 AGN, 1 cluster of galaxies (XBSJ 141830.5+251052) and 2 X-ray emitting stars (XBSJ 014100.6-675328 and XBSJ 123600.7-395217). Two X-ray sources (XBSJ 080411.3+650906 and XBSJ 110050.6-344331) are still unidentified at the time of this writing. The redshift of the 62 AGN are reported in Table 1 along with their basic X-ray spectral properties that will be used in this paper (e.g. photon index, intrinsic absorbing column density N_H , intrinsic 2-10 keV luminosity). A full account of the X-ray spectral properties for all the sources in the XMM-Newton Bright Survey will be reported in a forthcoming paper.

2.1. Absorption properties

The intrinsic 2-10 keV luminosities versus intrinsic absorption column densities for the HBSS AGN sample are shown in Figure 1. We have directly measured the intrinsic absorbing column density for 34 AGN while for the remaining 28 AGN we have only an upper limit. However the measured upper limits are such that we can easily divide the sample into absorbed and unabsorbed AGN using a value of $N_H = 4 \times 10^{21} \text{ cm}^{-2}$. Assuming a Galactic A_V/N_H ratio of $5.27 \times 10^{-22} \text{ mag cm}^{-2}$ (Bohlin et al. 1978), $N_H = 4 \times 10^{21} \text{ cm}^{-2}$ corresponds to $A_V \sim 2$; as shown and discussed in Caccianiga et al. (2008) (e.g. see their Figure 6) an A_V value of $\sim 2 \text{ mag}$ seems to be the best dividing value between optically type 1 (Sey1, Sey1.5, QSO, NLSy1) and optically type 2 (Sey1.8, Sey1.9, Sey2, QSO2) AGN in the XBS survey. Therefore, the choice of $N_H = 4 \times 10^{21} \text{ cm}^{-2}$ as dividing line between X-ray absorbed and unabsorbed AGN has a direct physical link to the optical classification. Three objects (XBS J041108.1-711341, XBS J205635.2-044717 and XBS J220601.5-015346) have an upper limit between $N_H = 4 \times 10^{21} \text{ cm}^{-2}$ and $N_H \sim 7 \times 10^{21} \text{ cm}^{-2}$ (see Figure 1), so the current X-ray data does not allow a firm classification as absorbed or unabsorbed AGN. On the other hand these three objects are classified as broad line (Type 1) AGN in the optical domain (Caccianiga et al. 2008); based on their optical properties these three objects will be considered here as unabsorbed AGN. With these choices the sample of unabsorbed (or marginally absorbed) AGN is composed of 40 objects while the sample of absorbed AGN is composed of 22 objects. As shown in Section 4 the specific choice of the

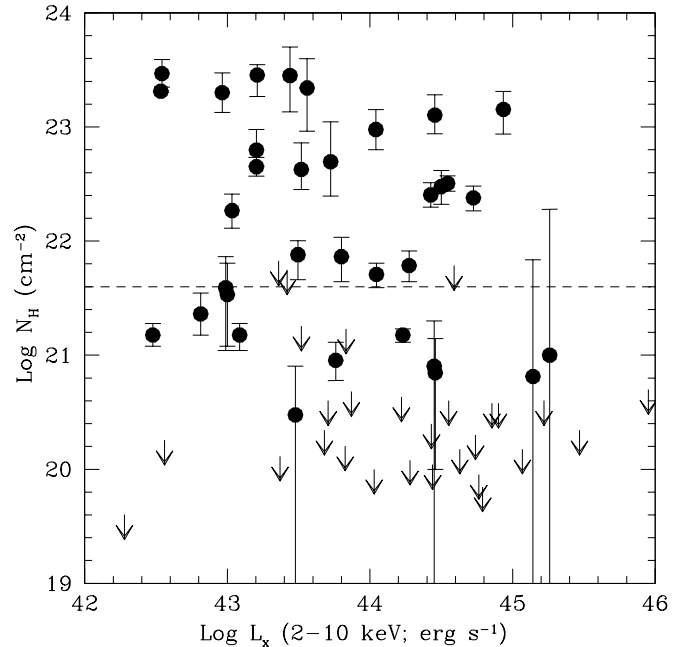


Fig. 1 Intrinsic 2-10 keV luminosity versus intrinsic absorption column densities N_H (both quantities derived from a complete X-ray spectral analysis) for the AGN belonging to the HBSS sample (filled circles: objects for which we have measured the N_H ; downward arrows: objects for which we have only an upper limit on N_H).

dividing line between absorbed and unabsorbed AGN does not affect the main results reported in this paper.

For the sake of clarity we will call in this paper as *unabsorbed AGN* those AGN with an intrinsic absorbing column density N_H below $4 \times 10^{21} \text{ cm}^{-2}$, as *absorbed AGN* those objects with N_H between 4×10^{21} and $\approx 10^{24} \text{ cm}^{-2}$ and as *Compton Thick AGN* those sources with N_H above 10^{24} cm^{-2} .

At the flux limit of the HBSS survey the measured surface densities of absorbed (unabsorbed) AGN is $0.87^{+0.23}_{-0.18}$ ($1.59^{+0.25}_{-0.25}$) deg^{-2} and the observed fraction of absorbed AGN is $37 \pm 7\%$. If we split the sample according to an intrinsic luminosity of $10^{44} \text{ erg s}^{-1}$ we have that the fraction of absorbed AGN is $29^{+10}_{-9}\%$ in the high luminosity regime and $42^{+11}_{-10}\%$ in the low luminosity regime, thus confirming first results based on a complete sub-sample of 28 HBSS objects fully identified reported in Caccianiga et al. (2004). However this crude comparison between low and high luminosity AGN is biased since it does not take into account selection effects due to the absorption, i.e. we can observe unobscured sources within a larger volume compared to the obscured ones since the intrinsic luminosity of the latter sources is depressed by photoelectric absorption. We will derive and discuss the unbiased intrinsic fraction of absorbed AGN as a function of the intrinsic X-ray luminosity in section 4.

It is worth noting that the selection strategy of the HBSS survey is extremely efficient in finding type 2 QSO, i.e. absorbed AGN with an intrinsic luminosity above $10^{44} \text{ erg s}^{-1}$. We have 9 of these sources in the HBSS sample (7 with

$N_H > 10^{22} \text{ cm}^{-2}$); they represent $15^{+6}_{-5}\%$ of the total AGN population and $41^{+13}_{-12}\%$ of the absorbed ones. At the flux limit of the HBSS survey the measured surface density of type 2 QSOs is $0.36^{+0.13}_{-0.12} \text{ deg}^{-2}$; this latter surface density of Type 2 QSO combined with the surface density of Type 2 QSOs reported in Perola et al. (2004) ($\sim 48 \text{ deg}^{-2}$ at a 2-10 keV flux limit of $\sim 10^{-14} \text{ erg cm}^{-2} \text{ s}^{-1}$) implies a slope in the integral LogN-LogS of Type 2 QSOs of ~ -2.1 between $\sim 10^{-13}$ and $\sim 10^{-14} \text{ erg cm}^{-2} \text{ s}^{-1}$.

Finally we have not found Compton Thick AGN, which are a fundamental population to produce the shape of the XRB around its emissivity peak ($\sim 30 \text{ keV}$, e.g. Gilli et al. 2007). As discussed in Appendix A even the 4.5-7.5 keV HBSS survey is quite inefficient in selecting this kind of AGN. Given their large flux depression due to the absorption, X-ray surveys above 10 keV are needed to select this kind of sources (see Della Ceca et al. 2007 for a recent review of this topic). We discuss Compton Thick AGN in Section 7 where we derive, in an indirect way, their X-ray luminosity function.

2.2. Redshift and Luminosity distribution

The redshift and intrinsic 2-10 keV luminosity distribution for the AGN belonging to the HBSS sample are reported in Figure 2 and Figure 3, respectively. The shaded histogram indicates the distribution for absorbed AGN while the empty histogram indicates the distribution for the unabsorbed ones. Both classes of AGN show a rather flat z distribution with the unabsorbed AGN population sampled up to $z \sim 1.5$ while the absorbed AGN population is sampled up to $z \sim 0.8$. Intrinsic 2-10 keV luminosities are distributed over 4 order of magnitude for the unabsorbed AGN population (from 10^{42} to $10^{46} \text{ erg s}^{-1}$ with a median logarithmic luminosity of ~ 44.2) and over about 2.5 order of magnitudes for the absorbed AGN population (from $\sim 7 \times 10^{42}$ to $10^{45} \text{ erg s}^{-1}$ with a median logarithmic luminosity of 43.7).

3. Cosmological properties

3.1. Evolution

For the sample of unabsorbed AGN (40 objects) we find that, according to the V_e/V_a test (Schmidt 1968; Avni & Bahcall 1980), the hypothesis of a uniform distribution of the objects in the Universe is rejected at a confidence level of $\sim 98\%$ ($\langle V_e/V_a \rangle = 0.616 \pm 0.046$). Assuming a pure luminosity evolution model with an evolutionary form $\propto (1+z)^C$ we find a best fit parameter of $C \approx 2.7$ with an associated 68% confidence interval of 1.9-3.0. This value of cosmological evolution is consistent, within the errors, both with the results obtained in the soft ($E \lesssim 3 \text{ keV}$) energy band using the *Einstein* Extended Medium Sensitivity Survey ($C = 2.56 \pm 0.17$; Maccacaro et al. 1991, Della Ceca et al. 1992) and the EMSS+Rosat AGN samples ($C = 2.6 \pm 0.1$; Page et al. 1997) and with the results in the 2-10 keV energy range reported in Ueda et al. (2003) ($C = 2.70^{+0.17}_{-0.25}$) and La Franca et al. (2005) ($C = 3.22^{+0.13}_{-0.26}$).

However it is now well established that a Luminosity Dependent Density Evolution (LDDE) model provides a better

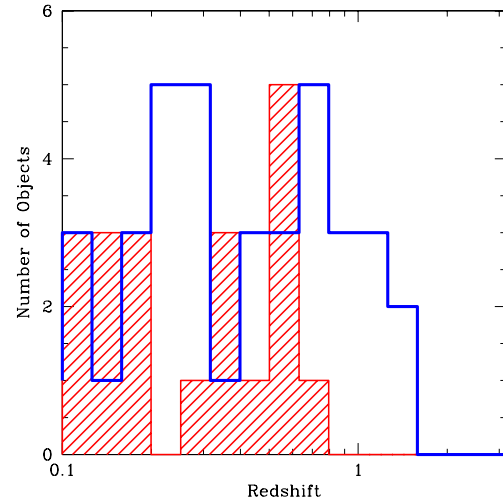


Fig. 2 Redshift distribution of the AGN belonging to the HBSS sample (shaded histogram: absorbed AGN; empty histogram: unabsorbed AGN)

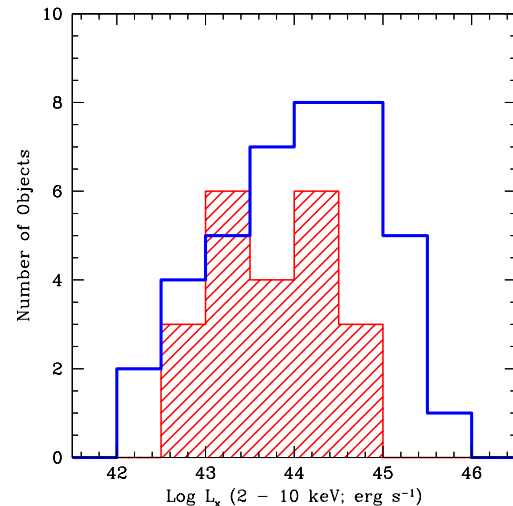


Fig. 3 Intrinsic 2-10 keV luminosity distribution of the AGN belonging to the HBSS sample (shaded histogram: absorbed AGN; empty histogram: unabsorbed AGN)

description of the evolutionary properties of AGN, both in the X-ray energy range (Hasinger et al. 2005; Ueda et al. 2003; La Franca et al. 2005; Silverman et al. 2007) and in the optical domain (Bongiorno et al. 2007).

To test this evolutionary behavior, we assume here an LDDE model with the parametrization as introduced by Ueda et al. (2003),

$$\frac{d\Phi(L_x, z)}{d\text{Log}L_x} = \frac{d\Phi(L_x, 0)}{d\text{Log}L_x} \times e(z, L_x)$$

$$e(z, L_x) = \begin{cases} (1+z)^{p1}, & (z < z_c) \\ e(z_c, L_x)[(1+z)/(1+z_c)]^{p2}, & (z \geq z_c) \end{cases}$$

$$z_c(L_X) = \begin{cases} z_c^*, & (L_X \geq L_a) \\ z_c^*(L_X/L_a)^\alpha & (L_X < L_a). \end{cases}$$

where z_c corresponds to the redshift where the direction of the evolution changes sign. It is worth noting that z_c is a function of the intrinsic luminosity of the object; if we assume the best fit parameters of $p_2=-1.15$; $z_c^* = 2.49$; $\alpha=0.20$; $\text{Log } L_a=45.80$ (adapted to $H_0=65$) as reported in La Franca et al. (2005), then z_c is $\sim 0.7, 1.1, 1.7$ for AGN with $L_X \sim 10^{43}, 10^{44}, 10^{45}$ erg s $^{-1}$, respectively. Given the coverage in the luminosity-redshift plane of the HBSS unabsorbed AGN sample, for each luminosity the objects are below z_c , implying that we are unable to derive p_2 , z_c^* , α and $\text{Log}L_a$. For this reasons we have fixed them from La Franca et al. (2005) and we have used the V_e/V_a test to constrain p_1 .

We obtain a best fit $p_1=6.5$ with an associated 68% confidence interval of 3.5 - 10.0. The distribution of the derived V_e/V_a values is consistent with being uniformly distributed between 0 and 1 according to a KS test (KS probability $\sim 95\%$). We have also checked that, given the coverage of the luminosity-redshift plane of the HBSS AGN sample, the best fit p_1 is virtually insensitive to the other parameters of the model; i.e., p_1 does not change by varying all the other parameters within their 1σ range as derived from La Franca et al. (2005).

The derived best fit value for p_1 is consistent, within the errors, with that reported in La Franca et al. (2005) ($p_1=4.62 \pm 0.26$) and is in very good agreement with those recently obtained, in the optical domain, by Bongiorno et al. (2007) using a sample of 130 broad line AGN with redshift up to $z=5$ from the VIMOS-VLT Deep Survey ($p_1=6.54$) and from Hopkins et al. (2007) using a large data set of AGN selected in the Mid-IR, optical, soft X-ray and hard X-ray ($p_1=5.95 \pm 0.23$).

Because of their number statistics (22 objects in total) and their distribution in the $L_X - z$ plane the cosmological evolution is unconstrained for the absorbed AGN sample (note that the absorbed AGN are sampled only up to $z \sim 0.8$). Therefore in the following, and in line with the Unification Scheme of AGN, we will make the assumption that this class of sources evolve with cosmic time (and within the redshift range sampled at the HBSS flux limit) in a similar way as the unabsorbed ones.

3.2. X-ray Luminosity Functions of Absorbed and Unabsorbed AGN

In this section we will derive the *intrinsic* (i.e. corrected for the selection bias due to the intrinsic absorption) local X-ray luminosity function of absorbed and unabsorbed AGN. For comparison with other survey projects the XLF will be derived in the 2-10 keV energy range using the $1/V_a$ method (Avni & Bahcall 1980) as follows.

For each AGN we have computed the maximum redshift (z_{max}) at which the source (characterized by the observed count rate in the 4.5-7.5 keV energy band, by the X-ray spectral shape and by the redshift) can still be detected above the MOS2 count rate limit of the HBSS sample ($= 2 \times 10^{-3}$ cts/s in the 4.5-7.5 keV band). The X-ray spectral shape of each AGN, as derived

from the X-ray spectral analysis (reported in Table 1), has been used to take properly into account k-corrections.

This z_{max} combined with the solid angle covered by the HBSS survey (25.17 deg^{-2}) and the best fit LDDE model described in the previous section allow us to compute, for each object i , the *density-weighted volume* V'_a (see Avni & Bahcall 1980)

$$V'_{ai} = 25.17 \times \int_0^{z_{max}} e(z, L_X) \times dV/dz \times dz$$

The XLFs computed using these volumes are the so called de-evolved XLF at $z=0$.

In order to obtain the differential 2-10 keV X-ray luminosity function we bin the individual contributions in bins of equal logarithmic width $\Delta \text{Log}L_X$ according to the intrinsic 2-10 keV luminosity as derived from the X-ray spectral analysis of each source. For each luminosity bin we have

$$\frac{d\Phi}{d\text{Log}L_x} = \sum_{i=1}^n \left[\frac{1}{V'_{ai} \Delta \text{Log}L_x} \right]$$

where n is the number of objects in that bin. Poissonian errors bars have been computed using the Gehrels (1986) prescription.

In summary, in the XLF computation we have used:

- the observed count rate in the selection 4.5-7.5 keV band, the count rate limit of the HBSS survey and the best fit LDDE model in estimating the *available* co-moving density weighted volume V'_{ai} of each source. The spectral shape of each individual source, as derived from the X-ray spectral analysis, has been used to properly take into account k-corrections;
- the intrinsic (2-10 keV) luminosities (as derived from the X-ray spectral analysis of each source) to divide the sources into luminosity bins.

In Appendix A we discuss a few simulations we have carried out to prove the validity of this approach.

In Figure 4 we show (filled dots) a binned representation of the de-evolved (2-10 keV) XLF obtained using the total AGN HBSS sample (62 objects). The derived XLF (at $z=0$) is compared with the 2-10 keV XLF obtained using *local* AGN samples, the latter being independent from cosmological evolution. In particular in Figure 4 we compare our XLF with that obtained from Shinozaki et al. (2006) using the 2-10 keV selected AGN in the HEAO1 survey (49 objects in total, dashed line) and by Sazonov & Revnivtsev (2004) using the 3-20 keV selected AGN sample (95 AGN in total; solid line) in the Rossi X-ray Timing Explorer (RXTE) slew survey. This last XLF has been converted from the 3-20 keV to the 2-10 keV energy range using a power-law model with photon index equal to 1.9 ($\frac{L_{2-10\text{keV}}}{L_{3-20\text{keV}}} = 0.8$). As can be seen in Figure 4 the best fit AGN XLF (at $z=0$) derived here is in excellent agreement with that derived using the RXTE slew data while its normalization is a factor between 2.5 to 5 times below that derived using the HEAO1 AGN sample (Shinozaki et al. 2006). This discrepancy in the normalization of the local (2-10 keV) XLFs was already discussed by Sazonov & Revnivtsev (2004) and by Shinozaki et al. (2006) and it is currently an open issue. It is worth noting that a similar shift between our computation of the

Table 2 Best Fit Parameters of the 2-10 keV XLF

| Sample | Objects | Log A | Log L_\star | γ_1 | γ_2 | KS-prob |
|----------------|---------|-------------------------|---------------|------------------------|------------------------|------------------|
| (1) | (2) | (3) | (4) | (5) | (6) | (7) |
| Unabsorbed AGN | 40 | $-6.21^{+0.12}_{-0.12}$ | 44.0 (fixed) | $1.08^{+0.19}_{-0.19}$ | $2.38^{+0.17}_{-0.18}$ | 0.44; 0.24; - |
| Absorbed AGN | 22 | $-6.62^{+0.17}_{-0.16}$ | 44.0 (fixed) | $1.55^{+0.31}_{-0.24}$ | $2.61^{+0.45}_{-0.52}$ | 0.10; 0.49; 0.34 |

Columns are as follows: (1) Sample; (2) number of objects in the sample; (3) XLF normalization, A, is in units of $h_{65}^3 \text{ Mpc}^{-3}$; (4) XLF break luminosity L_\star in units of $h_{65}^{-2} \text{ erg s}^{-1}$. Since L_\star is not well constrained we have fixed it to $10^{44} \text{ erg s}^{-1}$ close to that found for the total AGN population in Sazonov & Revnivtsev (2004) ($L_\star = 10^{43.6} \text{ erg s}^{-1}$) and in Shinozaki et al. (2006) ($L_\star = 10^{44.02} \text{ erg s}^{-1}$); (5) low-luminosity XLF slope; (6) high-luminosity XLF slope; (7) the three values are the probabilities (1D-KS test) that the observed z , L_x and, in the case of absorbed AGN, N_H distributions are consistent with being derived from the the best fit XLF plus cosmological evolution plus intrinsic N_H distribution derived here. See section 3.2 for details.

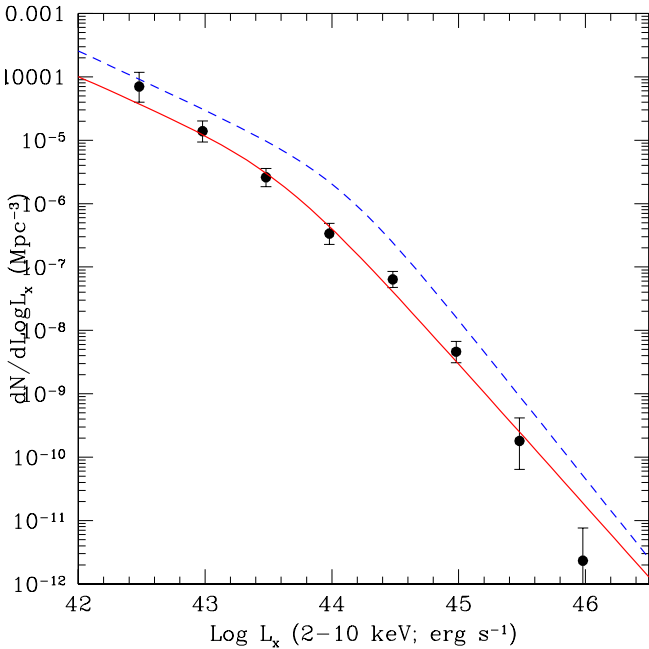


Fig. 4 De-evolved ($z=0$) X-ray luminosity function (2-10 keV) obtained using the total HBSS AGN sample (filled circles). We have also reported for comparison the local XLF for the total AGN population as derived by Shinozaki et al. (2006) (HEAO1 AGN sample; dashed line) and by Sazonov & Revnivtsev (2004) (RXTE AGN sample; solid line). See section 3.2 for details.

XLF and the Shinozaki et al. (2006) XLF is also present when we consider only the unabsorbed AGN population, suggesting that the possible different distribution of the absorption properties of the two samples cannot explain the different observed normalizations of the XLFs. Despite the different normalizations the shapes of the different XLFs seem to be in satisfactory agreement.

More important is the comparison between the XLF of the absorbed and unabsorbed AGN population in the HBSS sample reported in Figure 5 (unabsorbed population: open circles; absorbed population: filled circles). It is clear that the two populations are characterized by two different XLF with the absorbed AGN population being described by a steeper XLF, if compared with the unabsorbed ones, at all luminosities. The

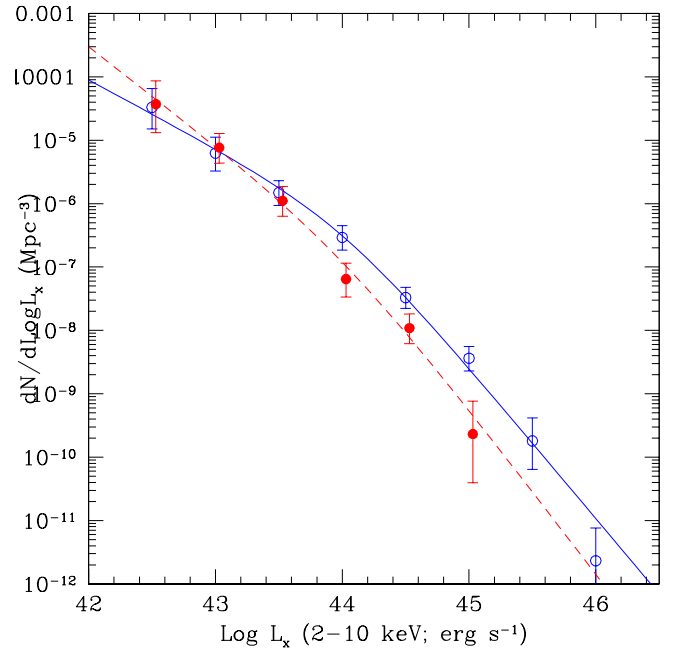


Fig. 5 Comparison between the de-evolved ($z=0$) X-ray luminosity function (2-10 keV) for the unabsorbed ($N_H < 4 \times 10^{21} \text{ cm}^{-2}$; open circles) and absorbed ($4 \times 10^{21} < N_H \leq 10^{24} \text{ cm}^{-2}$; filled circles) AGN in the HBSS sample. The solid and dashed lines represent the best fit two power-law function of the unabsorbed and absorbed AGN XLF, respectively (best fit parameters as reported in Table 2). Please note that for comparison reasons the XLF of absorbed AGN has been computed with a small shift ($\Delta \text{Log } L_x = 0.03$) with respect to that of unabsorbed AGN. See section 3.2 for details.

binned representation of the XLFs reported in Figure 5 have been fitted by a smoothly connected two power-laws function of the form

$$\frac{d\Phi(L_x, z=0)}{d\text{Log } L_x} = A \left[\left(\frac{L_x}{L_\star} \right)^{\gamma_1} + \left(\frac{L_x}{L_\star} \right)^{\gamma_2} \right]^{-1}$$

taking into account the error bars of each data point and by minimizing χ^2 using the routines in the QDP³ software package. Best fit XLF parameters and 1σ errors are reported in Table 2.

³ See in <http://heasarc.gsfc.nasa.gov/docs/software>

For the unabsorbed AGN population the value of γ_1 and γ_2 are consistent, within the errors, with those reported in Sazonov & Revnivtsev (2004) and in Shinozaki et al. (2006). For the absorbed AGN population the γ_1 (γ_2) derived here is slightly steeper (flatter) than that reported in Shinozaki et al. (2006) ($\gamma_1 = 1.12^{+0.17}_{-0.19}$; $\gamma_2 = 3.34^{+0.90}_{-0.65}$). Sazonov & Revnivtsev (2004) does not quote the XLF parameters for the absorbed AGN population.

As discussed in section 2 two HBSS sources (XBSJ080411.3+650906 and XBSJ110050.6-344331) are still unidentified at the time of this writing. Can their inclusion in the AGN sample substantially change the results discussed above? In particular their inclusion could be important if these sources were high luminosity absorbed AGN where we measure a deficit of absorbed sources. To answer to this question we have examined in detail their X-ray spectral properties as well as the optical (photometric) properties of the most likely optical counterpart. XBSJ110050.6-344331 is well described (fixing $z=0$) by a power-law model having $\Gamma = 1.80 \pm 0.16$ and $N_H = 1 \pm 0.5 \times 10^{21} \text{ cm}^{-2}$. Its 2-10 keV X-ray flux ($\sim 3 \times 10^{-13} \text{ erg cm}^{-2} \text{ s}^{-1}$), optical magnitude ($m_R = 18.0$), X-ray to optical flux ratio ($X/O \sim 1$) and X-ray spectral properties strongly suggest a type 1 (unabsorbed) object. On the contrary XBSJ080411.3+650906 is most likely an absorbed AGN. Its X-ray spectra is described (at $z=0$) by a power-law model having $\Gamma = 1.7 \pm 0.4$ and $N_H = 8.4 \pm 4.3 \times 10^{21} \text{ cm}^{-2}$, so with an intrinsic N_H (at the source z) well above $4 \times 10^{21} \text{ cm}^{-2}$. The optical magnitude of the counterpart ($m_R = 21.10$) combined with its 2-10 keV X-ray flux ($\sim 2.1 \times 10^{-13} \text{ erg cm}^{-2} \text{ s}^{-1}$) implies an X/O flux ratio of ~ 17.5 , strongly supporting the absorbed AGN hypothesis (e.g. Severgnini et al. 2006). If we use the relationship between X/O flux ratio and intrinsic luminosity reported in Fiore et al. (2003) the most likely redshift of this object is ~ 0.55 (consistent with a poor quality optical spectrum of the optical counterpart) and its intrinsic luminosity is $L_x \simeq 1.9 \times 10^{44} \text{ erg s}^{-1}$. The addition of this object to the HBSS absorbed AGN sample produce an increase of $\sim 8\%$ of the space density of the absorbed AGN population at $L_x \simeq 10^{44} \text{ erg s}^{-1}$, a very marginal difference that is well within the error bar reported in Figure 5. It is also worth noting that there are four objects (see Figure 1) which have a best fit N_H value below $4 \times 10^{21} \text{ cm}^{-2}$ but with error bars crossing this N_H dividing line. The two objects (having large error bars) with a luminosity around $2 \times 10^{45} \text{ erg s}^{-1}$ are optically classified as broad line QSO; so their optical properties are fully consistent with the unabsorbed classification. The two objects with a luminosity around $1 \times 10^{43} \text{ erg s}^{-1}$ are instead optical elusive AGN (Caccianiga et al. 2007a) and their unabsorbed classification was based on their best fit N_H value. On the other end their inclusion in the absorbed AGN sub-sample will increase the difference between absorbed and unabsorbed AGN around $L_x \simeq 10^{43} \text{ erg s}^{-1}$ strengthening our conclusions of different XLF of the two populations. To conclude, the results presented and discussed in this section are stable also taking into account all the uncertainty about the two unidentified sources and about our present classification (absorbed or unabsorbed AGN) break down. Finally, as consistency test, we have compared the observed z , L_x and N_H

distributions with those predicted by the best fit cosmological evolution model derived here (XLF + cosmological evolution) folded with the N_H distribution discussed in section 5. The 1D-KS probabilities reported in Table 2 confirms the goodness of our modeling of the AGN cosmological properties.

4. The intrinsic fraction of absorbed AGN

One of the most important open issues regarding absorbed AGN is to understand their relevance amongst the AGN population and if (and how) the fraction (F) of absorbed AGN changes as a function of L_x and z . We define F as the intrinsic ratio between the AGN with N_H in the range $4 \times 10^{21} - 10^{24} \text{ cm}^{-2}$ and all the AGN with N_H below 10^{24} cm^{-2} . This is a long standing issue coming back to almost 26 years ago when Lawrence & Elvis (1982) reported an anti-correlation between the intrinsic luminosity of the AGN and the presence of absorption. This issue has been recently re-discussed in many papers with contradicting results: several studies suggest that F decreases with L_x and increase with z (e.g. La Franca et al. 2005; Treister & Urry 2006), while other studies suggest that F is independent of L_x and z (e.g. Dwelly & Page 2006) or that F is dependent from L_x but not from z (e.g. Ueda et al. 2003; Akylas et al. 2006, Gilli et al. 2007). Having computed the intrinsic de-evolved XLFs of absorbed and unabsorbed AGN we can now use them to derive F. We stress that using the derived XLFs we should be free from the selection bias due to the absorption since the appropriate corrections have been already taken into account in the computation of the XLF itself. We also recall that we are not considering here Compton Thick AGN, so the derived F ratio is indeed a lower limit to the *true* fraction of absorbed AGN. Compton Thick AGN will be discussed in section 7.

Using the integral representation of the derived XLFs we have first computed F for AGN having an intrinsic luminosity above $\sim 3 \times 10^{42} \text{ erg s}^{-1}$ (i.e. around the luminosity of the faintest obscured AGN in the HBSS sample). The fraction ($F = 0.57 \pm 0.11$) is in excellent agreement with that found using hard ($E > 10 \text{ keV}$) selected (local) samples of AGN from INTEGRAL/Swift surveys at a flux limit of $\sim 10^{-11} \text{ erg cm}^{-2} \text{ s}^{-1}$. This comparison is reported in Table 3, where we have listed the value of F in the HBSS sample, in the SWIFT/BAT sample (Markwardt et al. 2005, Ajello et al. 2008) and in the INTEGRAL samples (Beckmann et al. 2006; Bassani et al. 2006). Please note that the local INTEGRAL/Swift samples are almost free from selection bias related to the absorption at least for N_H up to 10^{24} cm^{-2} . The good agreement implies that, after selection effect due to the absorption have been taken into account, the HBSS is sampling at a $f_x \sim 10^{-13} \text{ erg cm}^{-2} \text{ s}^{-1}$, the same population of absorbed AGN as the present surveys performed at $E > 10 \text{ keV}$. It is also worth noting that after selection effect have been taken into account the fraction of obscured AGN increases from an observed value of 0.37 ± 0.07 (see section 2.1) to an intrinsic ones of 0.57 ± 0.11 .

The differential fraction F of absorbed AGN as a function of the intrinsic luminosity is reported in Figure 6 left panel (solid line); we have also reported the 1σ error bar on F (vertical solid

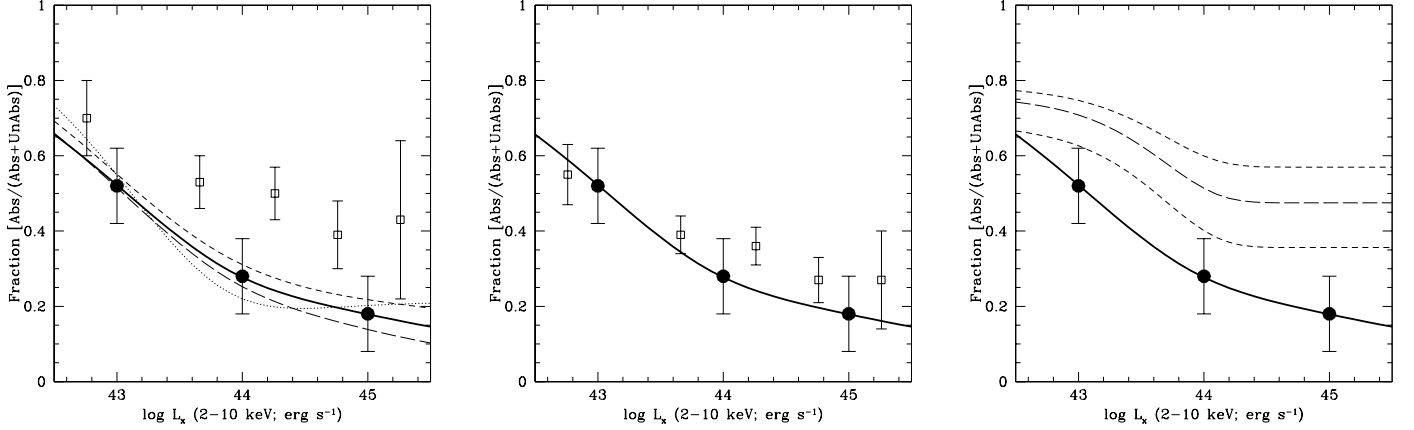


Fig. 6 *Left panel*: the thick solid line represents the differential fraction F of absorbed AGN as a function of the intrinsic luminosity obtained using the best fit de-evolved XLF of absorbed (N_H between 4×10^{21} and 10^{24} cm^{-2}) and unabsorbed (N_H below $4 \times 10^{21} \text{ cm}^{-2}$) AGN in the HBSS survey. The 68% confidence errors on this ratio are also reported at $L_x = 10^{43}, 10^{44}, 10^{45} \text{ erg s}^{-1}$. We have also reported the differential fraction of absorbed AGN obtained assuming no cosmological evolution (short dashed line), a cosmological evolution of the absorbed/unabsorbed ratio similar to that recently proposed by Treister & Urry (2006) (long dashed line) and that obtained using $N_H = 10^{22} \text{ cm}^{-2}$ as dividing value between absorbed and unabsorbed AGN (dotted line). The open squares represent the fraction of absorbed AGN as derived from Akylas et al. (2006). *Middle panel*: solid line as in the left panel. The Akylas et al. (2006) points have been rescaled to $z=0$ using the mean redshift in each luminosity bin and an evolution of the absorbed/unabsorbed ratio similar to that recently proposed by Treister & Urry (2006). *Right panel*: solid line as in the left panel. The long dashed line is the prediction from Gilli et al. (2007) on the synthesis model of the CXB. The two dashed lines enclose the uncertainty on the F ratio based on the CXB modeling. We stress that all the quantities reported in this figure refer to AGN with absorbing column density N_H below 10^{24} cm^{-2} . See section 4 for details.

Table 3 Fraction of absorbed AGN with $L_x \gtrsim 3 \times 10^{42} \text{ erg s}^{-1}$ in different samples¹

| Sample | F | NOTE |
|-------------------------|-----------------|-----------|
| HBSS | 0.57 ± 0.11 | XMM |
| Markwardt et al. (2005) | 0.59 ± 0.09 | SWIFT/BAT |
| Beckmann et al. (2006) | 0.54 ± 0.10 | INTEGRAL |
| Bassani et al. (2006) | 0.56 ± 0.09 | INTEGRAL |
| Ajello et al. (2008) | 0.57 ± 0.13 | SWIFT/BAT |

Notes: ¹ In deriving, from the original papers, the above reported quantities we have considered, as for the HBSS AGN sample, only the Compton Thin AGN ($N_H < 10^{24} \text{ cm}^{-2}$) and a dividing N_H line between absorbed and unabsorbed AGN fixed at $4 \times 10^{21} \text{ cm}^{-2}$. We have not reported the INTEGRAL results from Sazonov et al. (2007) since these authors do not report the absorbing column densities of their objects but simply split the objects into absorbed and unabsorbed according to an N_H value of 10^{22} cm^{-2} ; for comparison the fraction of absorbed AGN found from their sample using this N_H value is 0.42 ± 0.09 .

line at $L_x = 10^{43}, 10^{44}, 10^{45} \text{ erg s}^{-1}$), computed taking into account the current uncertainties on the XLFs.

Given the coverage in the luminosity-redshift plane of the HBSS AGN sample the results reported in Figure 6 are quite stable, i.e. they do not depend strongly on the value of the cosmological evolution parameter. To prove this in Figure 6 (left panel) we have also reported F as a function of L_x if we assume no cosmological evolution for absorbed and unabsorbed AGN

(short dashed line) or if we assume a cosmological evolution of the absorbed population faster than that the unabsorbed ones according to the Treister & Urry (2006) model ($F \propto (1+z)^{0.4}$; long dashed line). Finally we have also reported (dotted line) the fraction of absorbed AGN if we re-perform all the analysis but this time splitting the objects as absorbed or unabsorbed using $N_H = 10^{22} \text{ cm}^{-2}$ as dividing value (44 unabsorbed AGN, 18 absorbed AGN).

In the same left panel of Figure 6 we have also reported the fraction of obscured AGN as recently computed by Akylas et al. (2006) using a sample of AGN selected in the hard 2-8 keV band down to a flux limit of $6 \times 10^{-16} \text{ erg cm}^{-2} \text{ s}^{-1}$ (open squares), about a factor one hundred below our flux limit. The data points computed by Akylas et al. (2006) have been corrected for the different volumes sampled from absorbed and unabsorbed AGN (due to the absorption) in a similar way as done here. Although the HBSS sample and the Akylas et al. (2006) show a similar trend of decreasing F as a function of the intrinsic luminosity, the fractions computed at $z=0$ using the HBSS sample are systematically below (\sim a factor 2 for $L_x > 10^{43} \text{ erg s}^{-1}$) than those reported in Akylas et al. (2006). However the data points reported in Akylas et al. (2006) have been computed without taking into account possible differences in the cosmological evolution properties of the absorbed and unabsorbed AGN population. This effect, that we have already shown as of the second order for the HBSS AGN sample, could be very important for the Akylas et al. (2006) sample since their objects are at a significantly higher z compared to

the HBSS AGN sample. To test this effect in Figure 6 (middle panel) the Akylas et al. (2006) points have been rescaled to $z=0$ using the mean redshift in each luminosity bins (T. Akylas, private communication) and a cosmological evolution of F according to the model proposed by Treister & Urry (2006) ($F \propto (1+z)^{0.4}$). A much better agreement with our results is clearly evident, suggesting a possible evolution of the fraction of absorbed AGN with the redshift.

Finally in Figure 6 (right panel) we compare F with that required to produce the cosmic X-ray background according to the new synthesis model reported in Gilli et al. (2007) (long dashed line: best fit; short dashed lines: one σ error range; both computed and predicted F ratios refer only to absorbed AGN with N_H below 10^{24} cm^{-2}); we discuss this comparison in section 8.

5. The intrinsic N_H distribution in AGN

A second important and debated issue on the AGN astrophysics is related to their intrinsic N_H distribution, i.e. the N_H distribution of the AGN family computed taking into account the selection effects related to the photoelectric absorption. To compute this distribution we have proceeded as follows. We have first split the HBSS AGN sample in four bins of absorbing column densities up to $N_H = 10^{24} \text{ cm}^{-2}$ ($N_H = 10^{20} - 10^{21}$; $10^{21} - 10^{22}$; $10^{22} - 10^{23}$; $10^{23} - 10^{24} \text{ cm}^{-2}$). Second, we have computed the integral luminosity function using the objects in each bin of N_H and the $1/V_a$ method as discussed in Section 3.2. Third, using these XLFs we have determined the density of objects in each N_H bin having a luminosity above $\sim 3 \times 10^{42} \text{ erg s}^{-1}$ (i.e. around the luminosity of the faintest absorbed AGN in the HBSS sample). Finally in order to obtain the N_H distribution (reported in Figure 7 upper panel, as solid line) the density in each N_H bin has been normalized to the total density of AGN with N_H between 10^{20} and 10^{24} cm^{-2} . One σ Poisson error bars have been computed using the Gehrels (1986) prescription and the objects in each bin of N_H . It is now interesting to compare the rather flat $\text{Log} N_H$ distribution obtained from the HBSS sample with other samples of AGN or with that required from the synthesis model of the CXB. In Figure 7 (upper panel) we compare the N_H distribution derived using the HBSS sample with that computed using hard ($E > 10 \text{ keV}$) selected (local) sample of AGN from SWIFT/BAT and INTEGRAL surveys at a flux limit of $\sim 10^{-11} \text{ erg cm}^{-2} \text{ s}^{-1}$. We stress again that these latter samples are virtually free from selection bias related to the absorption for N_H below $\simeq 10^{24} \text{ cm}^{-2}$. Clearly the flat N_H distribution derived using the HBSS AGN sample is in agreement with that derived using local samples of X-ray selected AGN at a flux limit about a factor 100 higher, thus suggesting that we are indeed sampling a similar population of Compton Thin AGN. The derived flat $\text{Log} N_H$ distribution is also consistent with the flat $\text{Log} N_H$ distribution assumed by La Franca et al. (2005) in the cosmological analysis of the HELLAS2XMM AGN sample. Finally in Figure 7 (lower panel) we compare the N_H distribution derived here with that required by Gilli et al. (2007) (up to $N_H = 10^{24} \text{ cm}^{-2}$) to fit the spectra of the CXB; the current CXB synthesis modeling based on absorbed and unabsorbed AGN require an increasing

fraction of absorbed AGN that is clearly at odd with the results reported here.

It is worth noting that the flat $\text{Log} N_H$ distribution derived here is also markedly different from that derived by Risaliti et al. (1999) using a sample of optically selected Seyfert 2 galaxies, with the optically selected sample requiring an increasing fraction of absorbed AGN with increasing the N_H . This difference is expected and is due to the fact that we are considering in Figure 7 both optically type 1 and optically type 2 AGN, thus providing the N_H distribution of the total AGN population. A good agreement with Risaliti et al. (1999) is indeed obtained if we consider only the HBSS optically Type 2 AGN. In other words the $\text{Log} N_H$ distribution reported in Risaliti et al. (1999) does not represent the N_H distribution of the total AGN population but is probably more typical of that of optically selected Seyfert 2 galaxies, which, with few exceptions, are absorbed sources with N_H usually above 10^{22} cm^{-2} .

6. Comparison with AGN Unification Models

The results on the fraction of absorbed AGN as a function of the intrinsic luminosity discussed in section 4 can be now directly compared with the prediction(s) of the unification model of AGN. These results are inconsistent with the simplest unified scheme, where a similar thick molecular torus (at a distance of the order of one parsec from the central black hole) surrounds all the AGN, and which predicts that F is independent from L_x ; a modifications to this simple zero order unification scheme is clearly required. In Figure 8 (upper panel) we compare F - L_x relationship derived here with that expected in the framework of the original *receding torus model* ($F \propto L^{-0.5}$, dotted line; Lawrence 1991) and in the framework of the *radiation-limited clumpy dust torus* ($F \propto L^{-0.25}$, dashed line; Hönic & Beckert 2007); both these models have been normalized with our results at $L_x = 10^{43} \text{ erg s}^{-1}$. It is clearly evident the excellent agreement between our results and the prediction of the radiation-limited dusty torus discussed in Hönic & Beckert (2007).

Finally in Figure 8 (lower panel) we compare the F - L_x relationship from the HBSS sample with the AGN absorption model recently discussed by Lamastra et al. (2006). According to this model the absorption seen in Compton Thin AGN is not related to the obscuring torus but to molecular gas in a disk located far away from the X-ray source (between 25 and 450 pc depending on the BH mass). As shown in Lamastra et al. (2006) the anti-correlation between the ratio of absorbed AGN and the luminosity can be reproduced if a) there is a sufficient number of molecular clouds within the radius where the BH gravitational influence is dominant and b) there is a statistical correlation between the BH mass and the AGN luminosity. We have reported in Figure 8 (lower panel) as dashed lines the expected behavior of the fraction of absorbed AGN for values of the central surface densities of molecular clouds (from bottom to top) of 40, 80, 120, 200 and $400 M_\odot/\text{pc}^2$ as reported in Figure 4 (right panel) of Lamastra et al. (2006)⁴, based on the assumption $L_{\text{Bol}}/L_{\text{Edd}} = 0.1$ and luminosity dependent-

⁴ A. Lamastra has kindly provided us the expected behavior of their model for $L_x \gtrsim 3 \times 10^{44} \text{ erg s}^{-1}$.

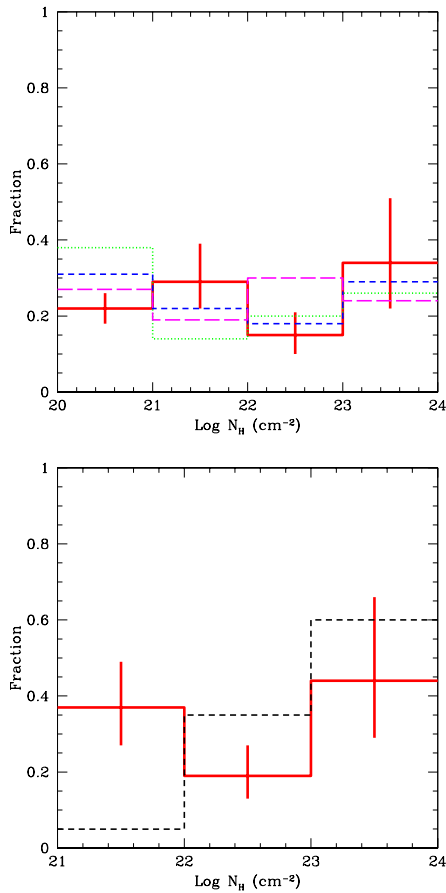


Fig. 7 *Upper panel*: intrinsic N_H distribution between 10^{20} and 10^{24} cm^{-2} obtained using the HBSS AGN sample (see section 5 for details), compared with N_H distribution from the SWIFT/BAT sample (Markwardt et al. 2005: long dashed line) and from the INTEGRAL samples (Beckmann et al. 2006: short dashed line; Bassani et al. 2006: dotted line). *Lower panel*: intrinsic N_H distribution between 10^{21} and 10^{24} cm^{-2} obtained using the HBSS AGN sample, compared with that required from the synthesis model of the CXB (Gilli et al. (2007)). In this panel, as done in Gilli et al. 2007, the number of objects in each N_H bin is normalized to the total number of AGN with N_H between 10^{21} and 10^{24} cm^{-2} .

bolometric corrections (see Lamastra et al. 2006 for details). Our results on the F- L_x relationship are fully consistent with this model if the surface density of molecular clouds in the central part of the galaxy is between 80 and 200 M_\odot/pc^2 , a condition that, as discussed in Lamastra et al. (2006) is consistent with the observations of local galaxies.

7. The X-ray luminosity function of Compton Thick AGN

As discussed above (and as done so far in this paper) XMM-Newton and *Chandra* data can be efficiently used to investigate the statistical properties of AGN with column densities below $\sim 10^{24}$ cm^{-2} . On the contrary the statistical properties (e.g. XLF) of absorbed sources having N_H above $\sim 10^{24}$ cm^{-2} , the so

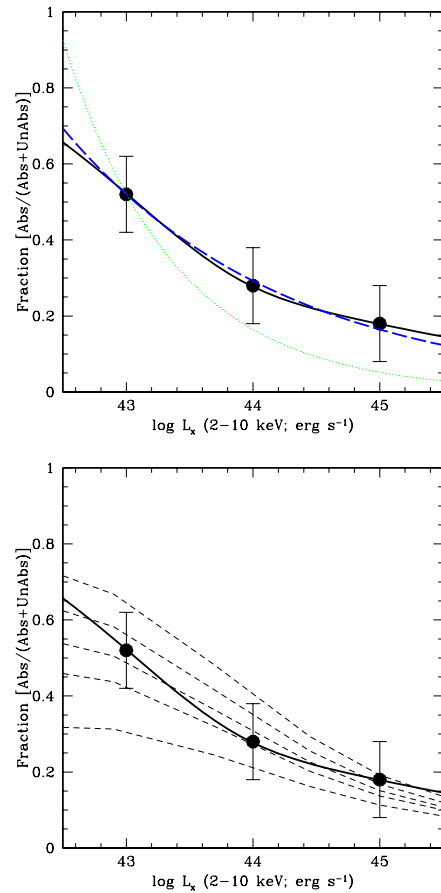


Fig. 8 *Upper panel*: the thick solid line represents the fraction F of absorbed AGN as a function of the intrinsic luminosity obtained using the best fit de-evolved XLF of absorbed (N_H between 4×10^{21} and 10^{24} cm^{-2}) and unabsorbed (N_H below 4×10^{21} cm^{-2}) AGN in the HBSS sample. The 68% confidence errors on this ratio are also reported at $L_x = 10^{43}, 10^{44}, 10^{45}$ erg s^{-1} . The dotted line represents the absorbed fraction expected from the original receding torus model discussed in Lawrence (1991) ($F \propto L^{-0.5}$), while the dashed line represents the absorbed fraction expected from the radiation-limited dusty torus recently discussed in Hönig & Beckert (2007) ($F \propto L^{-0.25}$); these expected fractions have been normalized to the observed values at $L_x = 10^{43}$ erg s^{-1} ; *Lower panel*: the thick solid line as in the upper panel. The dashed lines represent the expected behavior of the fraction of absorbed AGN for values of the galaxy central surface densities (from bottom to top) of 40, 80, 120, 200 and 400 M_\odot/pc^2 according to the models discussed in Lamastra et al. (2006).

called Compton Thick AGN, are currently completely unconstrained. According to the latest versions of synthesis modeling of the XRB (Gilli et al. 2007), these sources should represent a substantial fraction of the total AGN population but only a few dozens of them (mostly local) have been found and studied so far in the X-ray domain (see Della Ceca et al. 2007 for a review).

In Figure 9 we show the fraction of optically narrow line AGN as a function of the X-ray luminosity (dashed line) as de-

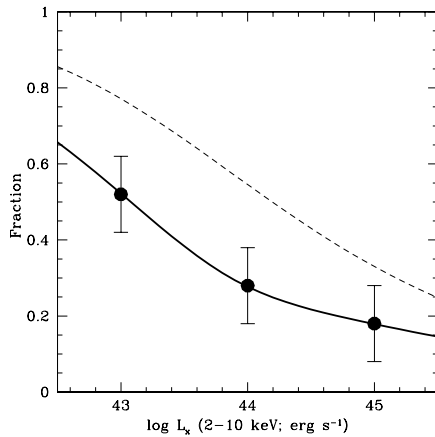


Fig. 9 The dashed line represents the fraction of optically narrow line AGN ($F_{optical}$) as derived by Simpson (2005) using a complete, magnitude-limited, sample of active galaxies from the Sloan Digital Sky Survey and assuming the mean $L_{[OIII]}/L_{(2-10keV)}$ ratio for Seyfert galaxies derived by Mulchaey et al. (1994). The thick solid line represents the fraction F of absorbed AGN (sources with N_H between 4×10^{21} and 10^{24} cm^{-2} divided by the sources with N_H below 10^{24} cm^{-2}) as a function of the intrinsic luminosity obtained using the best fit de-evolved XLF of absorbed and unabsorbed AGN in the HBSS sample. The 68% confidence errors on this ratio are also reported at $L_x = 10^{43}$, 10^{44} , 10^{45} erg s^{-1} .

derived by Simpson (2005) using a complete, magnitude-limited, sample of active galaxies from the Sloan Digital Sky Survey and assuming the mean $L_{[OIII]}/L_{(2-10keV)} \approx 0.015$ ratio for Seyfert galaxies obtained by Mulchaey et al. (1994) (fully consistent with the similar value reported in Heckman et al. 2005 for the unobscured view of Seyfert galaxies, $L_{[OIII]}/L_{(2-10keV)} \approx 0.017$). The thick solid line (and the error bars) are the results derived here on the fraction of absorbed ($4 \times 10^{21} < N_H \lesssim 10^{24}$ cm^{-2}) AGN obtained using the HBSS AGN sample (see Section 4); we recall here that in the HBSS we are sampling only AGN with N_H below 10^{24} cm^{-2} .

The behavior of the fraction of optically narrow line AGN derived by Simpson (2005) is remarkable similar to the correlation between F and L_x found here. More important, since the Simpson (2005) sample should contain both Compton Thin ($N_H \lesssim 10^{24}$ cm^{-2}) and Compton Thick ($N_H \gtrsim 10^{24}$ cm^{-2}) AGN (see also the results discussed in Heckman et al. 2005), the comparison between the results found by Simpson (2005) (dashed line in Figure 9; $F_{optical}$ hereafter) and those found here (solid line in Figure 9) allow us to estimate the ratio between Compton Thick AGN and AGN with N_H between 4×10^{21} and $\sim 10^{24}$ cm^{-2} as a function of the luminosity.

Assuming that the number of Compton Thick AGN is proportional to the number of AGN with N_H in the range $[4 \times 10^{21}; \sim 10^{24}$ $\text{cm}^{-2}]$, $N_{Thick} = C \times N_{4E21-E24}$, thus from the comparison between F and $F_{optical}$, and recalling that the definition of F given in Section 4 does not include Compton thick

AGN in either the numerator or denominator, we can derive

$$C = \frac{(F_{optical} - F)}{F \times (1 - F_{optical})}.$$

In order to derive an estimate of the density of Compton Thick AGN as a function of the luminosity we have first computed C for three values of the intrinsic X-ray luminosity ($L_x = 10^{43}$, $L_x = 10^{44}$ and $L_x = 10^{45}$ erg s^{-1}); thus we have multiplied them for the corresponding XLF of absorbed AGN with N_H between 4×10^{21} and $\sim 10^{24}$ cm^{-2} (i.e. second line of Table 2). The obtained results are reported in Figure 10 as open squares (the errors have been computed taking into account the errors reported in Figure 9).

These estimates of the density of Compton Thick AGN at $L_x = 10^{43}$, $L_x = 10^{44}$ and $L_x = 10^{45}$ erg s^{-1} can be well reproduced assuming an XLF similar, in shape, to that of absorbed AGN reported in Table 2 but having a normalization $A_{Thick} = 2 \times A_{4E21-E24}$; this XLF is shown as a thick solid line in Figure 10 while the two dashed lines corresponds to the XLFs with $A_{Thick} = A_{4E21-E24}$ (lower dashed line) and $A_{Thick} = 4 \times A_{4E21-E24}$ (upper dashed line).

In Figure 10 we have also reported:

a) the density of local Compton Thick AGN (filled circles at $L_x \sim 3 \times 10^{42}$ and $\sim 3 \times 10^{43}$ erg s^{-1}) as derived using the three Compton Thick AGN (NGC 4945, NGC 3281 and MKN 3) in the INTEGRAL all sky survey at $|b| > 5^\circ$ (Sazonov et al. 2007)⁵. To convert the observed 17-60 keV fluxes into 2-10 keV intrinsic (i.e. unabsorbed) luminosities we have corrected the fluxes for intrinsic absorption and assumed $\Gamma = 1.9$;

b) the density of Compton Thick AGN with $L_x \sim (1 - 4) \times 10^{43}$ erg s^{-1} (filled triangle) as derived by Daddi et al. (2007) using *Spitzer* and *Chandra* data in two GOODS fields with multiwavelengths information. Their estimated space density at z between 1.4 and 2.5 has been rescaled to $z=0$ using our best fit evolutionary model;

c) the density of Compton Thick AGN (filled squares) with $L_x \sim (3 - 10) \times 10^{43}$ erg s^{-1} (z between 0.7 and 1.0) and $L_x \sim (1 - 10) \times 10^{45}$ erg s^{-1} (z between 1.3 and 2.0) as derived by Fiore et al. (2008) using the *Spitzer* and *Chandra* data in the COSMOS field. Their estimated space density has been rescaled to $z=0$ using our best fit evolutionary model.

As it is clear in Figure 10 the different estimates of the space density of Compton Thick AGN, derived using different selection criteria (and methods), are in remarkably good agreement with the suggested XLF of Compton Thick AGN ($\gamma_1 = 1.55$, $\gamma_2 = 2.61$, $\text{Log } L_* = 44$, $\text{Log } A_{Thick} = -6.32$) with a possible hint of a XLF flattening below few times 10^{42} erg s^{-1} (where, we point out, the XLF of absorbed AGN in the HBSS is not well defined since we have no objects in the sample).

The good agreement seem to suggest that, at the sampled X-ray luminosities, the space density of optically *elusive* Compton Thick AGN (e.g. objects like Arp 299, see Della Ceca et al. 2002) is, at most, similar to that of optically selected Compton Thick AGN since the former population

⁵ We thank S. Sazonov to have provided us the sky coverage of this survey in a tabular form.

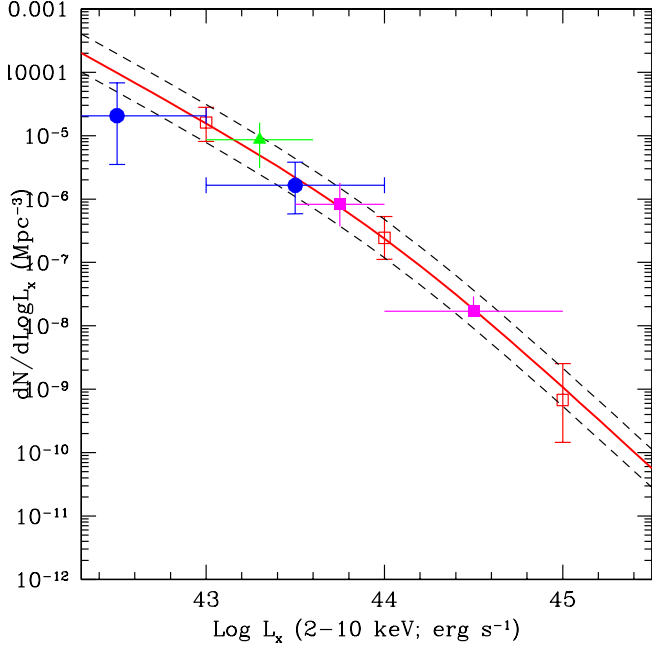


Fig. 10 The open squares represent the density of Compton Thick AGN at $L_X = 10^{43}$, 10^{44} and 10^{45} erg s $^{-1}$ derived as explained in section 7. The thick solid line represents the proposed XLF of Compton Thick AGN with $A_{Thick} = 2 \times A_{4E21-E24}$ ($\gamma_1 = 1.55$, $\gamma_2 = 2.61$, $\text{Log } L_\star = 44$, $\text{Log } A_{Thick} = -6.32$) while the two dashed lines corresponds to the XLFs with $A_{Thick} = A_{4E21-E24}$ (lower dashed line) and $A_{Thick} = 4 \times A_{4E21-E24}$ (upper dashed line). The filled circles at $L_{(2-10\text{keV})} \sim 3 \times 10^{42}$ and $\sim 3 \times 10^{43}$ erg s $^{-1}$ represent the density of local Compton Thick AGN derived using the Compton Thick AGN in the INTEGRAL all sky survey at $|b| > 5^\circ$. The filled triangle represents the density of Compton Thick AGN with $L_X \sim (1 - 4) \times 10^{43}$ erg s $^{-1}$ as derived by Daddi et al. (2007). The filled squares represent the density of Compton Thick AGN with $L_X \sim (3 - 10) \times 10^{43}$ erg s $^{-1}$ and $L_X \sim (1 - 10) \times 10^{45}$ erg s $^{-1}$ as derived by Fiore et al. (2008). The densities of Compton Thick AGN reported in Daddi et al. (2007) and Fiore et al. (2008) have been rescaled to $z=0$ using our best fit evolutionary model. See section 7 for details.

should be clearly missing in the optically selected sample of active galaxies defined in Simpson (2005) but should be present in the infrared or X-ray selected samples. This fact is also supported by the consideration that the total number of Compton Thick AGN cannot be increased arbitrarily but we have to take into account the limits imposed by the local black mass density derived by Marconi et al. (2004) from dynamical studies of local galaxy bulges ($\rho_{BH} = 4.0_{-1.2}^{+1.6} h_{65}^2 \times 10^5 M_\odot \text{Mpc}^{-3}$ for $H_0=65$). Using the formalism described in La Franca et al. (2005) (see their equations 15, 16 and 17), assuming a radiative efficiency ~ 0.1 , a bolometric conversion factor equal to 25 (Pozzi et al. 2007) and integrating the XLFs of AGN (unabsorbed, absorbed and Compton Thick) from $z=4.5$ to $z=0$ and from $L_X \sim 3 \times 10^{42}$ erg s $^{-1}$ to $\sim 10^{49}$ erg s $^{-1}$, the limit of $\rho_{BH} = 5.6 h_{65}^2 \times 10^5 M_\odot \text{Mpc}^{-3}$ is violated if the XLF of

Compton Thick AGN is more the ~ 4 times that of absorbed AGN, e.g. the upper envelope reported in Figure 10; we stress that this is probably an upper envelope since we have not considered in the computation of the local black mass density the objects with luminosity below $\sim 3 \times 10^{42}$ erg s $^{-1}$.

Finally the comparison of $F_{optical}$ and F reported in Figure 9 can be used to evaluate the ratio, Q , between Compton Thick and Compton Thin ($N_H < 10^{24}$ cm $^{-2}$) AGN. Assuming, as above, that the number of Compton Thick AGN is proportional to the number of AGN with N_H in the range $[4 \times 10^{21}; \sim 10^{24}$ cm $^{-2}]$, thus

$$Q = \frac{(F_{optical} - F)}{(1 - F_{optical})}.$$

We derive that the density ratio between Compton Thick AGN and Compton Thin AGN decreases from $Q = 1.08 \pm 0.44$ at $\sim 10^{43}$ erg s $^{-1}$ to $Q = 0.57 \pm 0.22$ at $\sim 10^{44}$ erg s $^{-1}$ to $Q = 0.23 \pm 0.15$ at $\sim 10^{45}$ erg s $^{-1}$.

8. Summary and Conclusions

We have discussed here the cosmological properties of the 62 AGN belonging to the XMM-Hard Bright Serendipitous Survey, a complete and representative sample of bright ($f_X \geq 7 \times 10^{-14}$ erg cm $^{-2}$ s $^{-1}$) serendipitous XMM-Newton sources selected in the 4.5 – 7.5 keV energy band on a sky area of ~ 25 deg $^{-2}$. Since the HBSS sample is almost completely spectroscopically identified (ID rate $\sim 97\%$) it allows us to have an unprecedented and unbiased view of the extragalactic 4.5 – 7.5 keV sky in the bright flux regime. Using an N_H dividing value of 4×10^{21} cm $^{-2}$ (see Section 2.1), the HBSS AGN sample is composed of 40 unabsorbed (or marginally absorbed) AGN and 22 absorbed AGN.

The main results reported and discussed in this paper are:

1. the HBSS survey is extremely efficient in finding type 2 QSO, i.e. absorbed AGN with an intrinsic luminosity in excess to 10^{44} erg s $^{-1}$. They represent $(15 \pm 6)\%$ of the total AGN population and $(41 \pm 13)\%$ of the absorbed ones. At the flux limit of the HBSS survey ($\sim 7 \times 10^{-14}$ erg cm $^{-2}$ s $^{-1}$ in the 4.5–7.5 keV energy range) the measured surface density of type 2 QSOs is $0.36_{-0.12}^{+0.13}$ deg $^{-2}$ ($0.28_{-0.10}^{+0.15}$ deg $^{-2}$ if we consider only the 7 Type 2 QSO with $N_H > 10^{22}$ cm $^{-2}$). At the same flux limit the measured surface density of absorbed (unabsorbed) AGN is $0.87_{-0.18}^{+0.23}$ ($1.59_{-0.25}^{+0.25}$) deg $^{-2}$ and the observed fraction of absorbed AGN is $(37 \pm 7)\%$;
2. the de-evolved ($z=0$) 2-10 keV X-ray luminosity function of the total AGN population derived using the AGN HBSS sample is in very good agreement with the local AGN XLF obtained by Sazonov & Revnivtsev (2004) using the data from the Rossi X-ray Timing Explorer survey. A smaller normalization (a factor between 2.5 to 5 times depending on L_X) is observed if compared with the local HEAO1 AGN XLF as recently computed from Shinozaki et al. (2006);
3. absorbed and unabsorbed AGN are characterized by two different XLF with the absorbed AGN population being described by a steeper XLF, if compared with the unabsorbed ones, at all luminosities;

4. the intrinsic fraction of absorbed AGN with $L_X \gtrsim 3 \times 10^{42}$ erg s⁻¹ (i.e. around the luminosity of the faintest absorbed AGN in the HBSS sample) is 0.57 ± 0.11 . This is in excellent agreement with that found using hard ($E > 10$ keV) selected (local) sample of AGN from INTEGRAL/Swift surveys at a flux limit of 10^{-11} erg cm⁻² s⁻¹;
5. the fraction F of absorbed AGN is a function of luminosity. A comparison of our results with those reported in Akylas et al. (2006) (obtained using a source sample at fainter fluxes and thus at higher z) seem to suggest an evolution of the fraction of absorbed AGN with z . This evolution is consistent with that recently proposed by Treister & Urry (2006);
6. we find a flat Log N_H distribution for N_H between 10^{20} and 10^{24} cm⁻², still in very good agreement with local samples of hard ($E > 10$ keV) selected AGN at a flux limit of 10^{-11} erg cm⁻² s⁻¹ .
7. the shape of the F- L_x relationship and the derived flat Log N_H distribution (both in good agreement with the assumptions and the results of La Franca et al. 2005) are not consistent with the current models for the production of the cosmic X-ray background based on the absorbed AGN. This disagreement, probably due to the fact that we are not sampling the X-ray source population producing the bulk of the CXB, may require a revision in the current model's parameters, e.g. an increase of the fraction of absorbed sources with redshift and/or a N_H distribution which depends on the source luminosity, redshift or both;
8. by comparing the results obtained here with the behavior of the fraction of optical narrow line AGN derived by Simpson (2005) using a complete, magnitude-limited, sample of active galaxies from the Sloan Digital Sky Survey we have derived, in an indirect way, the X-ray luminosity function of Compton Thick AGN; it is described by a smoothly connected two power-law function (see section 3.2) having $\gamma_1 = 1.55$, $\gamma_2 = 2.61$, $\text{Log } L_* = 44$, $\text{Log } A_{\text{Thick}} = -6.32$. The density ratio, Q , between Compton Thick AGN ($N_H \gtrsim 10^{24}$ cm⁻²) and Compton Thin AGN ($N_H \lesssim 10^{24}$ cm⁻²) decreases from $Q = 1.08 \pm 0.44$ at $\sim 10^{43}$ erg s⁻¹ to $Q = 0.57 \pm 0.22$ at $\sim 10^{44}$ erg s⁻¹ to $Q = 0.23 \pm 0.15$ at $\sim 10^{45}$ erg s⁻¹ ;
9. finally, the decreasing fraction of absorbed AGN as a function of the luminosity is fully consistent with the hypothesis of a reduction of the covering factor of the *gas* component as a function of the luminosity. A similar reduction with the luminosity of the covering factor of the circumnuclear *dust* component has been recently pointed out by Maiolino et al. (2007) using a sample of AGN observed with *Spitzer*. These results are clearly inconsistent with the simplest unified scheme of AGN. Indeed we found an excellent agreement between our results and the predictions of the radiation-limited dusty torus discussed in Hönig & Beckert (2007). An alternative model which also explains well our results has been recently discussed by Lamastra et al. (2006) and is based on the obscuration due to molecular gas in a disk located far away from the X-ray source (between 25 and 450 pc depending on the BH mass).

Acknowledgements. Based on observations made with: ESO Telescopes at the La Silla and Paranal Observatories; the Italian Telescopio Nazionale Galileo (TNG) operated on the island of La Palma by the Fundación Galileo Galilei of the INAF (Istituto Nazionale di Astrofisica); the Spanish Observatorio del Roque de los Muchachos of the Instituto de Astrofisica de Canarias; the German-Spanish Astronomical Center, Calar Alto (operated jointly by Max-PlanckInstitut für Astronomie and Instituto de Astrofisica de Andalucía, CSIC); XMM-Newton, an ESA science mission with instruments and contributions directly funded by ESA Member States and the USA (NASA). We thanks A. Lamastra, T.Akylas, R. Gilli and S. Sazonov to have provided us their results in a tabular form and A. Comastri, R. Gilli, F. La Franca and C. Perola for useful comments. Finally we sincerely thanks the anonymous referee for the useful comments that have substantially improved the paper. RDC, AC, TM and PS acknowledge financial support from the MIUR, grant PRIN-MUR 2006-02-5203 and from the Italian Space Agency (ASI), grants n. I/088/06/0 and n. I/023/05/0. FJC acknowledges financial support by the Spanish Ministry of Education and Science, through project ESP2006-13608-C01-01. This research has made use of the Simbad database and of the NASA/IPAC Extragalactic Database (NED) which is operated by the Jet Propulsion Laboratory, California Institute of Technology, under contract with the National Aeronautics and Space Administration.

References

- Ajello, M., et al. 2008, ApJ, 673, 96
Akylas, A., Georgantopoulos, I., Georgakakis, A., Kitsionas, S., & Hatziminaoglou, E. 2006, A&A, 459, 693
Avni, Y., & Bahcall, J. N. 1980, ApJ, 235, 694
Bassani, L., Malizia, A., Stephen, J. B., & for the INTEGRAL AGN survey team 2006, ArXiv Astrophysics e-prints, arXiv:astro-ph/0610455
Beckmann, V., Soldi, S., Shrader, C. R., Gehrels, N., & Produit, N. 2006, ApJ, 652, 126
Begelman, M. C. 2004, Coevolution of Black Holes and Galaxies, 374
Bohlin, R. C., Savage, B. D., & Drake, J. F. 1978, ApJ, 224, 132
Bongiorno, A., et al. 2007, A&A, 472, 443
Boyle, B. J., Shanks, T., & Peterson, B. A. 1988, MNRAS, 235, 935
Caccianiga, A., et al. 2004, A&A, 416, 901
Caccianiga, A., Severgnini, P., Della Ceca, R., Maccacaro, T., Carrera, F. J., & Page, M. J. 2007a, A&A, 470, 557
Caccianiga, A., et al. 2008, A&A, 477, 735
Cagnoni, I., Della Ceca, R., & Maccacaro, T. 1998, ApJ, 493, 54
Comastri, A., Setti, G., Zamorani, G., & Hasinger, G. 1995, A&A, 296, 1
Croom, S. M., Smith, R. J., Boyle, B. J., Shanks, T., Miller, L., Outram, P. J., & Loaring, N. S. 2004, MNRAS, 349, 1397
Daddi, E., et al. 2007, ApJ, 670, 173
Della Ceca, R., Maccacaro, T., Gioia, I. M., Wolter, A., & Stocke, J. T. 1992, ApJ, 389, 491
Della Ceca, R., Castelli, G., Braitto, V., Cagnoni, I., & Maccacaro, T. 1999, ApJ, 524, 674
Della Ceca, R., et al. 2002, ApJ, 581, L9
Della Ceca, R., et al. 2004, A&A, 428, 383.

- Della Ceca, R., et al. 2007, ArXiv e-prints, 709, arXiv:0709.3060
- Dwelly, T., & Page, M. J. 2006, MNRAS, 372, 1755
- Fabian, A. C., Barcons, X., Almaini, O., & Iwasawa, K. 1998, MNRAS, 297, L11
- Ferrarese, L., & Merritt, D. 2000, ApJ, 539, L9
- Fiore, F., La Franca, F., Giommi, P., Elvis, M., Matt, G., Comastri, A., Molendi, S., & Gioia, I. 1999, MNRAS, 306, L55
- Fiore, F., et al. 2003, A&A, 409, 79
- Fiore, F., et al. 2008, A&A, submitted
- Gehrels, N. 1986, ApJ, 303, 336
- Gilli, R., Comastri, A., & Hasinger, G. 2007, A&A, 463, 79
- Hasinger, G., Miyaji, T., & Schmidt, M. 2005, A&A, 441, 417
- Heckman, T. M., Ptak, A., Hornschemeier, A., & Kauffmann, G. 2005, ApJ, 634, 161
- Hönig, S. F., & Beckert, T. 2007, MNRAS, 380, 1172
- Hopkins, P. F., Richards, G. T., & Hernquist, L. 2007, ApJ, 654, 731
- Kormendy, J., & Richstone, D. 1995, ARA&A, 33, 581
- La Franca, F., et al. 2005, ApJ, 635, 864
- Lamastra, A., Perola, G. C., & Matt, G. 2006, A&A, 449, 551
- Lawrence, A., & Elvis, M. 1982, ApJ, 256, 410
- Lawrence, A. 1991, MNRAS, 252, 586
- López-Santiago, J., Micela, G., Sciortino, S., Favata, F., Caccianiga, A., Della Ceca, R., Severgnini, P., & Braito, V. 2007, A&A, 463, 165
- Maccacaro, T., Della Ceca, R., Gioia, I. M., Morris, S. L., Stocke, J. T., & Wolter, A. 1991, ApJ, 374, 117
- Madau, P., Ghisellini, G., & Fabian, A. C. 1994, MNRAS, 270, L17
- Magorrian, J., et al. 1998, AJ, 115, 2285
- Maiolino, R., Shemmer, O., Imanishi, M., Netzer, H., Oliva, E., Lutz, D., & Sturm, E. 2007, A&A, 468, 979
- Marconi, A., Risaliti, G., Gilli, R., Hunt, L. K., Maiolino, R., & Salvati, M. 2004, MNRAS, 351, 169
- Markwardt, C. B., Tueller, J., Skinner, G. K., Gehrels, N., Barthelmy, S. D., & Mushotzky, R. F. 2005, ApJ.Letters, 633, L77
- Miyaji, T., Hasinger, G., & Schmidt, M. 2001, A&A, 369, 49
- Mulchaey, J. S., Koratkar, A., Ward, M. J., Wilson, A. S., Whittle, M., Antonucci, R. R. J., Kinney, A. L., & Hurt, T. 1994, ApJ, 436, 586
- Page, M. J., Mason, K. O., McHardy, I. M., Jones, L. R., & Carrera, F. J. 1997, MNRAS, 291, 324
- Perola, G. C., et al. 2004, A&A, 421, 491
- Pozzi, F., et al. 2007, A&A, 468, 603
- Risaliti, G., Maiolino, R., & Salvati, M. 1999, ApJ, 522, 157
- Sazonov, S. Y., & Revnivtsev, M. G. 2004, A&A, 423, 469
- Sazonov, S., Revnivtsev, M., Krivonos, R., Churazov, E., & Sunyaev, R. 2007, A&A, 462, 57
- Schmidt, M. 1968, ApJ, 151, 393
- Severgnini, P., et al. 2006, A&A, 451, 859
- Setti, G. & Woltjer, L. 1989, A&A, 224, 21
- Shinozaki, K., Miyaji, T., Ishisaki, Y., Ueda, Y., & Ogasaka, Y. 2006, AJ, 131, 2843
- Simpson, C. 2005, MNRAS, 360, 565
- Silverman, J. D., et al. 2007, ArXiv e-prints, 710, arXiv:0710.2461
- Treister, E., & Urry, C. M. 2006, ApJ, 652, L79
- Ueda, Y., et al. 1998, Nature, 391, 866
- Ueda, Y., et al. 2003, ApJ, 598, 886

Table 1: Basic X-ray information of the XMM-Newton HBSS AGN Sample

| Source | Rate $\times 10^{-3}$ cts/s | z | Γ | N_H $\times 10^{22}$ cm $^{-2}$ | $f_{2-10keV}$ $\times 10^{-13}$ erg cm $^{-2}$ s $^{-1}$ | Log $L_{2-10keV}$ erg s $^{-1}$ |
|---------------------|-----------------------------------|-------|--|--|--|------------------------------------|
| (1) | (2) | (3) | (4) | (5) | (6) | (7) |
| XBSJ002618.5+105019 | 2.34 ± 0.55 | 0.473 | 2.02 ^{+0.07} _{-0.06} | < 0.011 | 2.83 | 44.44 |
| XBSJ013240.1-133307 | 3.23 ± 0.71 | 0.562 | 1.90 (frozen) | 2.540 ^{+0.710} _{-0.560} | 1.76 | 44.43 |
| XBSJ013944.0-674909 | 2.05 ± 0.46 | 0.104 | 1.94 ^{+0.14} _{-0.12} | < 0.018 | 1.15 | 42.56 |
| XBSJ015957.5+003309 | 3.80 ± 0.92 | 0.310 | 2.14 ^{+0.09} _{-0.09} | < 0.010 | 2.91 | 44.03 |
| XBSJ021640.7-044404 | 2.08 ± 0.49 | 0.873 | 2.24 ^{+0.08} _{-0.09} | < 0.020 | 1.11 | 44.74 |
| XBSJ021808.3-045845 | 2.67 ± 0.25 | 0.712 | 2.01 ^{+0.04} _{-0.04} | < 0.007 | 2.32 | 44.79 |
| XBSJ021817.4-045113 | 3.30 ± 0.40 | 1.080 | 1.84 ^{+0.04} _{-0.03} | < 0.040 | 2.65 | 45.22 |
| XBSJ021822.2-050615 | 4.54 ± 0.43 | 0.044 | 1.66 ^{+0.34} _{-0.36} | 20.540 ^{+0.360} _{-0.440} | 3.00 | 42.53 |
| XBSJ023713.5-522734 | 3.23 ± 0.61 | 0.193 | 1.90 ^{+0.18} _{-0.13} | < 0.180 | 2.74 | 43.52 |
| XBSJ030206.8-000121 | 3.10 ± 0.42 | 0.641 | 1.90 ^{+0.06} _{-0.06} | < 0.015 | 2.23 | 44.63 |
| XBSJ030614.1-284019 | 4.61 ± 0.92 | 0.278 | 1.56 ^{+0.26} _{-0.13} | < 0.048 | 2.91 | 43.87 |
| XBSJ031015.5-765131 | 4.39 ± 0.46 | 1.187 | 1.92 ^{+0.04} _{-0.04} | < 0.022 | 3.41 | 45.47 |
| XBSJ031146.1-550702 | 5.87 ± 1.12 | 0.162 | 2.08 ^{+0.13} _{-0.12} | < 0.013 | 2.79 | 43.37 |
| XBSJ031859.2-441627 | 2.16 ± 0.49 | 0.140 | 1.72 ^{+0.43} _{-0.37} | 0.390 ^{+0.340} _{-0.280} | 1.63 | 42.99 |
| XBSJ033845.7-352253 | 2.37 ± 0.36 | 0.113 | 1.90 (frozen) | 28.500 ^{+6.700} _{-10.000} | 1.67 | 43.21 |
| XBSJ040658.8-712457 | 3.41 ± 0.68 | 0.181 | 1.90 (frozen) | 21.970 ^{+17.670} _{-12.780} | 1.59 | 43.56 |
| XBSJ040758.9-712833 | 4.96 ± 0.91 | 0.134 | 1.90 (frozen) | 28.230 ^{+21.960} _{-14.640} | 2.56 | 43.44 |
| XBSJ041108.1-711341 | 2.20 ± 0.42 | 0.923 | 1.95 ^{+0.48} _{-0.36} | < 0.610 | 0.82 | 44.59 |
| XBSJ050536.6-290050 | 2.19 ± 0.44 | 0.577 | 1.85 ^{+0.20} _{-0.18} | 0.610 ^{+0.210} _{-0.170} | 1.33 | 44.27 |
| XBSJ052108.5-251913 | 2.11 ± 0.55 | 1.196 | 1.72 ^{+0.29} _{-0.19} | 0.100 ^{+1.800} _{-0.100} | 2.46 | 45.26 |
| XBSJ052128.9-253032 | 3.08 ± 0.88 | 0.588 | 1.90 (frozen) | 12.710 ^{+6.460} _{-3.980} | 1.34 | 44.45 |
| XBSJ074202.7+742625 | 3.38 ± 0.49 | 0.599 | 2.02 ^{+0.16} _{-0.15} | 0.070 ^{+0.070} _{-0.060} | 1.64 | 44.46 |
| XBSJ074312.1+742937 | 10.92 ± 0.64 | 0.312 | 1.99 ^{+0.06} _{-0.07} | < 0.040 | 9.67 | 44.55 |
| XBSJ083737.0+255151 | 2.98 ± 0.71 | 0.105 | 1.77 ^{+0.35} _{-0.33} | 0.340 ^{+0.300} _{-0.220} | 3.04 | 43.00 |
| XBSJ083737.1+254751 | 7.30 ± 1.12 | 0.080 | 1.92 ^{+0.14} _{-0.12} | 0.150 ^{+0.040} _{-0.040} | 6.63 | 43.09 |
| XBSJ091828.4+513931 | 3.03 ± 0.54 | 0.185 | 1.47 ^{+0.51} _{-0.30} | 4.240 ^{+3.030} _{-1.410} | 2.62 | 43.52 |
| XBSJ095218.9-013643 | 24.50 ± 2.98 | 0.020 | 1.90 (frozen) | 29.400 ^{+9.600} _{-7.000} | 11.00 | 42.54 |
| XBSJ101850.5+411506 | 2.16 ± 0.49 | 0.577 | 2.29 ^{+0.09} _{-0.05} | < 0.025 | 1.51 | 44.43 |
| XBSJ101922.6+412049 | 2.46 ± 0.47 | 0.239 | 2.13 ^{+0.28} _{-0.10} | < 0.040 | 2.87 | 43.71 |
| XBSJ104026.9+204542 | 8.70 ± 1.15 | 0.465 | 1.99 ^{+0.05} _{-0.05} | < 0.009 | 6.21 | 44.76 |
| XBSJ104522.1-012843 | 3.00 ± 0.67 | 0.782 | 2.05 ^{+0.11} _{-0.11} | < 0.038 | 2.11 | 44.85 |
| XBSJ104912.8+330459 | 2.06 ± 0.51 | 0.226 | 1.68 ^{+0.19} _{-0.17} | 0.030 ^{+0.050} _{-0.030} | 1.83 | 43.48 |
| XBSJ112026.7+431520 | 2.32 ± 0.37 | 0.146 | 1.65 ^{+0.83} _{-0.42} | 6.280 ^{+3.210} _{-1.730} | 1.87 | 43.20 |
| XBSJ113106.9+312518 | 2.27 ± 0.44 | 1.482 | 1.77 ^{+0.37} _{-0.26} | 0.065 ^{+0.620} _{-0.065} | 1.08 | 45.14 |
| XBSJ113121.8+310252 | 3.88 ± 0.69 | 0.190 | 1.62 ^{+0.10} _{-0.28} | 0.760 ^{+0.250} _{-0.300} | 2.70 | 43.50 |
| XBSJ113148.7+311358 | 3.43 ± 0.48 | 0.500 | 1.90 (frozen) | 3.200 ^{+0.540} _{-0.460} | 2.96 | 44.54 |
| XBSJ122656.5+013126 | 3.07 ± 0.54 | 0.733 | 1.61 ^{+0.23} _{-0.21} | 2.390 ^{+0.650} _{-0.550} | 2.23 | 44.73 |
| XBSJ124641.8+022412 | 2.22 ± 0.49 | 0.934 | 2.22 ^{+0.10} _{-0.10} | < 0.038 | 1.36 | 44.90 |
| XBSJ132038.0+341124 | 2.89 ± 0.40 | 0.065 | 1.77 ^{+0.13} _{-0.10} | 0.150 ^{+0.040} _{-0.030} | 2.54 | 42.48 |
| XBSJ133942.6-315004 | 3.52 ± 0.51 | 0.114 | 1.62 ^{+0.22} _{-0.18} | 0.230 ^{+0.120} _{-0.080} | 1.70 | 42.81 |
| XBSJ134656.7+580315 | 3.33 ± 0.56 | 0.373 | 1.90 (frozen) | 9.500 ^{+4.720} _{-3.160} | 1.47 | 44.04 |
| XBSJ134749.9+582111 | 7.39 ± 0.66 | 0.646 | 2.19 ^{+0.02} _{-0.03} | < 0.015 | 5.14 | 45.07 |
| XBSJ140102.0-111224 | 7.21 ± 0.59 | 0.037 | 1.90 ^{+0.04} _{-0.02} | < 0.004 | 5.21 | 42.28 |
| XBSJ140113.4+024016 | 2.10 ± 0.52 | 0.631 | 2.05 ^{+0.42} _{-0.24} | < 0.170 | 0.34 | 43.83 |
| XBSJ140127.7+025605 | 6.66 ± 0.62 | 0.265 | 1.57 ^{+0.05} _{-0.06} | 0.150 ^{+0.020} _{-0.020} | 7.42 | 44.23 |
| XBSJ141531.5+113156 | 2.58 ± 0.34 | 0.257 | 1.84 ^{+0.07} _{-0.05} | < 0.022 | 2.09 | 43.68 |
| XBSJ142741.8+423335 | 3.62 ± 0.53 | 0.142 | 1.90 (frozen) | 4.480 ^{+0.930} _{-0.770} | 2.11 | 43.20 |
| XBSJ143835.1+642928 | 3.57 ± 0.54 | 0.118 | 1.84 ^{+0.42} _{-0.18} | 1.850 ^{+0.730} _{-0.550} | 2.33 | 43.03 |
| XBSJ143911.2+640526 | 2.44 ± 0.39 | 0.113 | 1.90 (frozen) | 20.000 ^{+9.720} _{-6.560} | 1.09 | 42.96 |
| XBSJ153452.3+013104 | 8.36 ± 1.30 | 1.435 | 1.75 ^{+0.09} _{-0.04} | < 0.050 | 7.56 | 45.95 |

Table 1: continued.

| Source | Rate $\times 10^{-3}$ cts/s | z | Γ | N_H $\times 10^{22}$ cm^{-2} | $f_{2-10\text{keV}}$ $\times 10^{-13}$ $\text{erg cm}^{-2} \text{s}^{-1}$ | Log $L_{2-10\text{keV}}$ erg s^{-1} |
|---------------------|-----------------------------------|-------|------------------------|---|---|---|
| (1) | (2) | (3) | (4) | (5) | (6) | (7) |
| XBSJ160645.9+081525 | 7.36 ± 1.37 | 0.618 | $1.75^{+0.71}_{-0.71}$ | $14.270^{+6.290}_{-5.610}$ | 3.84 | 44.94 |
| XBSJ161820.7+124116 | 2.09 ± 0.61 | 0.361 | 1.90 (frozen) | $4.960^{+6.140}_{-2.480}$ | 0.88 | 43.72 |
| XBSJ165425.3+142159 | 5.26 ± 1.08 | 0.178 | $2.11^{+0.07}_{-0.03}$ | < 0.016 | 6.34 | 43.83 |
| XBSJ165448.5+141311 | 6.25 ± 1.79 | 0.320 | $1.84^{+0.13}_{-0.08}$ | < 0.043 | 4.46 | 44.22 |
| XBSJ193248.8-723355 | 4.47 ± 0.73 | 0.287 | $1.48^{+0.25}_{-0.22}$ | $0.730^{+0.350}_{-0.290}$ | 2.30 | 43.80 |
| XBSJ204043.4-004548 | 3.24 ± 0.80 | 0.615 | 1.90 (frozen) | $3.000^{+1.150}_{-0.900}$ | 1.66 | 44.50 |
| XBSJ205635.7-044717 | 2.08 ± 0.50 | 0.217 | $1.91^{+0.51}_{-0.35}$ | < 0.560 | 1.66 | 43.42 |
| XBSJ205829.9-423634 | 3.91 ± 0.56 | 0.232 | $1.91^{+0.09}_{-0.09}$ | $0.090^{+0.040}_{-0.030}$ | 3.17 | 43.76 |
| XBSJ213002.3-153414 | 2.30 ± 0.47 | 0.562 | $2.10^{+0.23}_{-0.21}$ | $0.080^{+0.120}_{-0.080}$ | 1.84 | 44.45 |
| XBSJ213820.2-142536 | 2.80 ± 0.59 | 0.369 | $1.61^{+0.13}_{-0.13}$ | $0.510^{+0.130}_{-0.120}$ | 2.26 | 44.05 |
| XBSJ214041.4-234720 | 3.30 ± 0.68 | 0.490 | $2.19^{+0.10}_{-0.10}$ | < 0.012 | 1.69 | 44.28 |
| XBSJ220601.5-015346 | 2.26 ± 0.55 | 0.211 | $1.56^{+0.16}_{-0.09}$ | < 0.670 | 1.66 | 43.36 |

Columns are as follows: (1) Source name; (2) Source MOS2 count rate, and 1σ error, in the 4.5-7.5 keV energy band (units of 10^{-3} cts/s). Please note that the reported count rates have been corrected for vignetting; (3) Redshift; (4) Source photon index, and 90% confidence errors; (5) Absorbing column density at the source redshift, and 90% confidence errors; (6) Observed 2-10 keV flux corrected for Galactic absorption; (7) Intrinsic (i.e. de-absorbed) 2-10 keV luminosity.

Appendix A: Computation of the intrinsic 2-10 keV XLF using the HBSS AGN sample

In Section 3 we have derived the intrinsic 2-10 keV XLF of absorbed and unabsorbed AGN using the HBSS AGN sample selected in the 4.5-7.5 keV energy band. To this purpose we have used the $1/V_a$ method, a well established procedure to derive space densities of interesting astronomical objects (Avni & Bahcall 1980).

However to apply this method to the absorbed AGN population the following considerations have to be taken into account. Given an intrinsic count rate (i.e. the count rate we would have observed without intrinsic absorption), the observed count rate is a function of the absorbing column density N_H (at the source redshift) and of the energy selection band. Therefore, a given source with an intrinsic count rate above the survey threshold could have been missed in the survey since, because of the absorption, its observed count rate falls below the survey count rate threshold.

In order to compute the z_{max} of each source (absorbed or not) in section 3 we have used the observed MOS2 count rate in the selection band (4.5-7.5 keV) and the count rate limit of the HBSS survey in the same energy band ($= 2 \times 10^{-3}$ cts/s). The intrinsic (2-10 keV) luminosities (as derived from the X-ray spectral analysis of each source) have been thus used to divide the sources into luminosity bins and to derive the luminosity function. A similar procedure was recently used by Shinozaki et al. (2006) in computing the local luminosity function of the absorbed and unabsorbed AGN in the HEAO1 surveys; however Shinozaki et al. (2006) did not prove the correctness of this approach and, in particular, if this approach may recover the *true* space density of the absorbed AGN population.

To investigate this aspect we have simulated a source sample assuming:

a) a 2-10 keV local luminosity function described by a smoothly connected two power-law function (see section 3.2) having the following parameters $\gamma_1 = 1.55$, $\gamma_2 = 2.61$, $\text{Log} L^* = 44$. These parameters are those describing the intrinsic 2-10 keV XLF of the absorbed AGN population in the HBSS survey;

b) a LDDE cosmological evolution model (see section 3.1) having best fit parameters as follows: $p_1=6.5$, $p_2=-1.15$, $z_c^* = 2.49$, $\alpha=0.20$, $\text{Log} L_a=45.80$;

c) a flat intrinsic $\text{Log} N_H$ distribution from 10^{20} to 10^{25} cm^{-2} .

Folding all this information together we have produced a simulated sample of ~ 40000 sources that would be visible at the count rate threshold of the HBSS survey. For each source we have computed the observed count rate in the 4.5-7.5 keV, the redshift, the absorbing column density N_H and the intrinsic luminosity in the 2-10 keV band. For simplicity we have assumed the same intrinsic photon index ($\Gamma = 1.9$) for all the sources. This simulated sample has been thus analyzed with the same procedure used for the real HBSS source sample, namely, using the observed 4.5-7.5 count rate (and the count rate limit of the HBSS survey), combined with the input LDDE model, to evaluate space densities and the intrinsic (2-10 keV) luminosities to split the sources into luminosity bins.

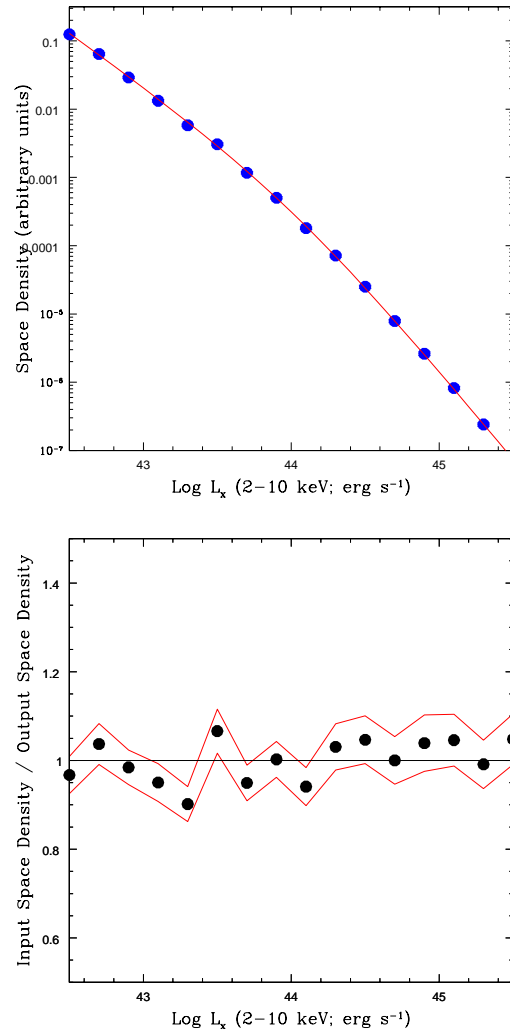


Fig. A.1 The results reported in this Figure are those relative to the sources filtered by an absorbing column density N_H between 10^{23} and 10^{24} cm^{-2} . *Upper panel*: comparison between the input XLF (solid line) and the XLF computed (dots) using the method discussed here. *Lower panel*: ratio between the input and output XLF. The solid lines enclose 1σ error bars on this ratio.

The results obtained for one extreme example (the sources having an absorbing column density in the range between 10^{23} and 10^{24} cm^{-2}) are shown in Figure A.1; we have reported the input XLF, the output XLF and the ratio between the derived XLF at $z=0$ from the simulated sample and the input local XLF. It is worth noting the very good agreement between the input and output XLF. Similar results have been obtained for less extreme values of the N_H . For the purpose of this paper the main conclusion we reached using these simulations is that for the HBSS selection band (4.5-7.5 keV) our approach to compute space densities can recover the *true* space density of the AGN population as a function of the intrinsic N_H up to $N_H \sim 10^{24} \text{ cm}^{-2}$, **even if** in the N_H bin between 10^{23} and 10^{24} about 50 % of the AGN are lost (i.e. observed count rate is below the survey threshold) because of the intrinsic absorption. Our simulations

also show that the above statement is not true for N_H above 10^{24} where a dramatic number of objects ($\sim 95\%$ between 10^{24} and 10^{25}) are lost because of absorption (note that for these high N_H values the situation could be even worst if Compton scattering is considered). In summary using the HBSS survey and our computation method we can recover the true space density of absorbed AGN up to $N_H \sim 10^{24} \text{ cm}^{-2}$, while we are quite inefficient in selecting AGN with an intrinsic N_H above this value. The shape of the intrinsic XLF, at least for AGN with N_H up to $\sim 10^{24} \text{ cm}^{-2}$, is therefore recovered allowing us to compare the XLF of absorbed and unabsorbed AGN consistently. We have repeated these simulations using different values of the parameters for the XLF and/or for the cosmological evolution obtaining the same results thus giving us confidence about the overall procedure.